

5-1-2014

Design of a Micro-Focus X-Ray Source Validated by Model Protein Crystals

Lavanya Ramachandran
University of Wisconsin-Milwaukee

Follow this and additional works at: <https://dc.uwm.edu/etd>

 Part of the [Electrical and Electronics Commons](#), and the [Physics Commons](#)

Recommended Citation

Ramachandran, Lavanya, "Design of a Micro-Focus X-Ray Source Validated by Model Protein Crystals" (2014). *Theses and Dissertations*. 482.
<https://dc.uwm.edu/etd/482>

This Thesis is brought to you for free and open access by UWM Digital Commons. It has been accepted for inclusion in Theses and Dissertations by an authorized administrator of UWM Digital Commons. For more information, please contact open-access@uwm.edu.

**DESIGN OF A MICRO-FOCUS X-RAY SOURCE
VALIDATED BY MODEL PROTEIN CRYSTALS**

by

Lavanya Ramachandran

A Thesis Submitted in
Partial Fulfillment of the
Requirements for the Degree of

Master of Science
in Engineering

at

The University of Wisconsin-Milwaukee

May 2014

ABSTRACT

DESIGN OF A MICRO-FOCUS X-RAY SOURCE VALIDATED BY MODEL PROTEIN CRYSTALS

by

Lavanya Ramachandran

The University of Wisconsin-Milwaukee, 2014
Under the Supervision of Professor Marius Schmidt

The main objective of this thesis was to build a Laboratory Microfocus X-ray Source for Protein Crystallography (LMXS-PC), an X-ray source that would provide prospective users programmatic control and remote capability.

A study of the crystal was conducted using Photoactive Yellow protein (PYP) and cytochrome c nitrite reductase (ccNiR). The instrument was then tested by mounting the crystal in the instrument and collecting data.

The other objective of my research work was to determine the crystal structure of PYP using X-ray crystallography techniques. I attempted many trials in PYP crystal in an effort to achieve a high-quality diffraction pattern; however, crystals diffract to less than 2 Å resolution limit. My interest in the crystal of Photoactive Yellow Protein to understand how electron density is obtained from the information contained within the diffraction patterns.

TABLE OF CONTENTS

1	Introduction	2
1.1	Background of X-ray crystallography	3
1.2	Theory of X-ray diffraction	4
1.3	Biological background	8
1.3.1	Photoactive Yellow Protein (PYP)	8
1.3.2	Cytochrome c nitrite reductase (ccNiR)	10
1.4	Overview of the X-ray crystallographic method	11
1.5	My contribution	12
	Materials and Methods	13
2.1	Setup of a self-designed micro-focus X-ray source	14
2.2	Hardware components of the X-ray source	15
2.2.1	Genix head	15
2.2.2	The control unit	16
2.2.3	Water-to-air chiller	16
2.2.4	Vacuum pump	17
2.2.5	AVT camera	17
2.2.6	SMC 9300 controller	18
2.2.7	Cryojet	18
2.2.8	MarCCD 165 detector	21

2.2.9	Fast shutter.....	23
2.2.10	Optical table.....	24
2.3	Software used to control hardware components	25
2.3.1	Software for X-ray control unit	25
2.3.2	Software for the SMC controller	26
2.3.3	SMC crystal alignment tools	27
2.3.4	Software for MarCCD	28
2.3.5	AVT camera software.....	30
2.4	Protein crystallization.....	30
2.4.1	Preparation of buffer solutions	30
2.4.2	Crystallization methods	30
2.5	Methods for mounting crystal	32
2.5.1	Cryoloop	32
2.5.2	Mitegen loop.....	33
2.5.3	Capillary mount	34
2.6	Data collection.....	35
2.6.1	PYP crystals mounted in a cryoloop.....	35
2.6.2	PYP crystals mounted in a mitegen loop.....	37
3.	Date reduction and analysis	38
3.1	Introduction	39

3.2	Data reduction	40
3.3	Phase determination	40
3.4	Crystallographic Object-Oriented Toolkit (COOT).....	41
3.5	Refmac	41
4	Results	43
4.1	X-ray diffraction pattern for PYP.....	44
4.2	X-ray diffraction pattern for ccNiR.....	45
4.4	Electron density map for PYP.....	47
4.4.1	Low temperature.....	47
4.4.2	Room temperature	48
5	Discussion	50
5.1	Discussion.....	52
5.2	Conclusion.....	52
6	References	53
7	Appendix	58

LIST OF FIGURES

Figure 1-1: Electromagnetic spectrum adapted from Prof.Paul R.Baumann, State university of New York.....	3
Figure 1-2: Ewald's sphere, adapted from (N.Purwar, 2013). An Ewald sphere of radius $1/\lambda$ (\AA^{-1}), 2θ is the scattering angle, \vec{H} is the scattering vector. The directions of incoming and scattered beam are represented by \vec{s}_0 and \vec{s}_1	7
Figure 1-3: PYP from Dr.Schmidt's lecture notes :(a) Ectohiorhodospira halophile, which lives in sunny, hypersaline lakes (b) Ribbon structure of Photoactive yellow protein (PYP).....	9
Figure 1-4: (a) ccNiR adapted from Matthew Youngblut, Evan T. Jud, and A. Andrew Pacheco, 2012 (ribbon representation)(b) Cytochrome c nitrite reductase (ccNiR) crystal mounted using a cryoloop with width of 250mm and length of 400mm.....	11
Figure 1-5: A bird's eye view of an X-ray experiment. The X-ray beam is produced by the source on the left hitting the crystal mounted on the goniometer. Scattered X-rays (diffracted and background) are detected on the charge coupled device (CCD) detector.	11
Figure 2-1: Components of microfocus X-ray source :(a) CT-Collimator Tube, BS-Beam Stop, SH-Shutter, TC-Temperature Control, G-Goniometer, C-Camera, S-Sample, D-Detector, OT- Optical Table, DP-Diffraction Pattern.....	14
Figure 2-2 : (a) Genix beam delivery system (b) The control unit (c) Water to air chiller (d) Vacuum pump (from the Genix manual).....	16
Figure 2-3: (a) SMC 9300 Motor controller (from the manual of the SMC controller) (b) Sideview of the AVT camera (from http://www.alliedvisiontec.com)	17
Figure 2-4: (a) The view from the top of the control unit and dewar head(from the cryojet manual),(b) Overall view of cryojet system (c) Cryojet controller front panel (from the cryojet manual) (d) Cryojet controller full details front panel(from Prof. Schmidt's lab)	19
Figure 2-5: Shows as the complete view of the MarCCD 165 detector.....	21
Figure 2-6: (a) Shutter controller(sc10) (b) SH05(shutter) (from Thorlabs).	23
Figure 2-7: Optical Table(from Thorlabs).....	24

Figure 2-8: Genix Utility software (screen shot)	25
Figure 2-9: (a) SMC software (b) SMC crystal alignment tool (screen shot).....	26
Figure 2-10: (a) MarCCD graphical user interface used to initial setup (b) MarCCD GUI that is used to collect single frame data (screen shot).....	28
Figure 2-11 : (a) GUI that is used to collect the complete data set,(b)Crystal Toolkit Software(screen shot).....	29
Figure 2-12: (a) The sitting-drop vapor diffusion method for protein crystallization (b)Crystallisation plate (picture from Hampton research).....	31
Figure 2-13: (a) Cryoloop properly installed in a magnetic mounting base (from the Hampton Research) (b) Crystal perfectly frozen in a cryoloop (c) Crystal imperfectly frozen (screen shot).....	32
Figure 2-14: (a) Schematic diagram of a room-temperature loop mounting technique (b) Photograph of the room-temperature mount (from Hampton Research).....	33
Figure 2-15: PYP crystal is inside the quartz glass capillary tube (screen shot).....	34
Figure 2-16: (a) Perfectly frozen crystal the length of crystal is 580mm (b) Perfectly frozen crystal width of crystal is 185mm (screen shot).....	35
Figure 2-17: (a) Crystal mounted by mitogen loop central with length of 390 mm and width of 105 mm (b) Crystal mounted by mitogen loop side view (screen shot).....	37
Figure 3-1: (a) Pyp crystal mounted by cryoloop (b) Diffraction pattern collected from the MarCCD detector (c) Electron density map	39
Figure 4-1: A typical diffraction pattern for a strongly diffracting crystal is shown on the left; the detected reflections are shown on the right. Each reflection is noted by a cross-hair, with red and yellow used to denote those reflections above and below the current threshold used for indexing, respectively.....	45
Figure 4-2: A typical diffraction pattern for a strongly diffracting crystal is shown on the left; the detected reflections are shown on the right. Each reflection is noted by a cross-hair, with red and yellow used to denote those reflections above and below the current threshold used for indexing, respectively.....	45
Figure 4-3: (a) Electron density map obtained using the COOT software for low temperature data set (b) Electron density map obtained using the COOT software for room temperature data set (screen shot).....	47

LIST OF TABLES

4.3.1 Table 1 :Data Statistics for PYP	46
7.8.1 Table 2 :Rotating X-ray anode generator.....	75
7.8.2 Table 3 :Synchrotron.....	76
7.8.3 Table 4 :Sealed tube.....	77

LIST OF ABBREVIATIONS

PYP - Photoactive yellow protein

CcNiR - Cytochrome c nitrite reductase

CCP4 - Collaborative Computational Project, Number 4, 1994

COOT - Crystallographic Object-Oriented Toolkit

SMC - Stepper Motor Controller

CCD - Charge coupled devices

TCP -Transmission Control Protocol

IP – Internet Protocol

TTL - Transistor-Transistor logic

LAN - Local area network

VNC - Virtual Network Computing

GUI - Graphical user interface

ARP - Auto Refinement process

APS-Advanced Photon Source

LMXS-PC-Laboratory Microfocus X-ray Source Protein Crystallography

ACKNOWLEDGMENTS

First and foremost, I would like to express my appreciation to Dr. Marius Schmidt, who has provided me with the opportunity to perform research in this field and supported me throughout my research with his patience and guidance. His wisdom, knowledge, and commitment to the highest standards inspired and motivated me in this field.

I would further like to thank each of my thesis committee members, Dr. Brian Armstrong and Dr. George Hanson. Every member of my committee has helped me in my discussions. Their efforts greatly advanced my graduate career.

Most of the results described in this thesis would not have been obtained without a close collaboration within laboratories. I would like to thank Dr Shaliesh Tripathi, University of Wisconsin-Milwaukee, who provided me with the PYP Crystal studied in this research and offered guidance in the biological side of the research that was invaluable to me. I am most grateful to Jason James Tenboer and Namrta Purwar, whose endless help and supports made this research possible and the research life pleasant.

Lastly and most importantly, my deepest gratitude goes to my family for their love and support, including my husband Rajarajan Muthukkannan, who has always supported, encouraged and believed in me throughout my life. I give my distinguished appreciation to my family especially my mother and father who pray for me throughout my life as well as my two sisters who encourage me to be strong and optimistic always.

Chapter 1

Introduction and Background

1 Introduction

In this thesis, I describe the design, development, and function of a Laboratory Microfocus X-ray Source for Protein Crystallography (LMXS-PC). This safe X-ray source provides programmatic control and remote capability so end users can control the X-ray source. A complete study of the instrument was conducted and explained in Chapter 2. To test its function, I used Photoactive Yellow Protein (PYP) and Cytochrome c nitrite reductase (ccNiR). PYP is a photoreceptor in bacteria. The ccNiR play an important role in reducing nitrite to ammonia. Due to their known structure, they can be used as model systems to demonstrate the functioning of X-ray instruments.

PYP, which is isolated from the phototrophic bacterium *Ectothiorhodospira halophila*, is a water-soluble protein whose three-dimensional X-ray crystallographic structure has been determined to high resolution and serves as a paradigm for structural studies of the interaction of light and proteins. CcNiR is a soluble protein found in the periplasm of several bacterial species such as *Schewanella oneidensis*. In order to obtain the diffraction patterns from the PYP and ccNiR crystals, I mounted them on the X-ray instrument using three different tools: cryoloops, mitogen loops and capillary tubes. The obtained diffraction data was analyzed using Imosflm, CCP4 (Collaborative Computational Project, Number 4, 1994); the calculated electron density was inspected using the program COOT (Crystallographic Object-Oriented Toolkit). The detailed procedure is explained in Appendix Section 7.

1.1 Background of X-ray crystallography

The electrons are then liberated from a heated filament and accelerated by high voltage towards the metal target (M. Wiener, 2008). X-rays are generated when electrons strike a metal target.

X-rays are a form of electromagnetic radiation, where wavelengths vary from 0.01 – 10 nm (1 – 100 Å) in the electromagnetic spectrum (Petrucci *et al.*, 2002). The corresponding frequencies fall in the range of 30 petahertz (3×10^{16}) to 30 exahertz (3×10^{19}) with energies in the range of 100 eV to 100 keV. The wavelengths (range shown in figure 1.1) are shorter than those of ultra violet (UV) rays and longer than those of gamma rays. X-rays with photon energies above 5-10 keV (below 0.2-0.1 nm) wavelength are called hard X-rays, while those with lower energy (600 eV) are called soft X-rays. Due to their penetrating ability, hard X-rays are widely used to image objects, for example in medical radiography and airport security. Since the wavelengths of hard X-rays are similar to the size of atoms, they are also useful for determining the 3D structure of proteins by X-ray scattering (M. Wiener, 2008).

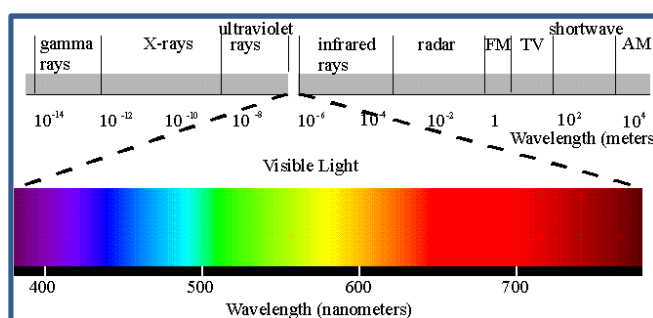


Figure 1-1: Electromagnetic spectrum adapted from Prof Paul R. Baumann, State university of New York.

The discovery of X-rays gave crystallographers a powerful tool that could see inside crystals. X-ray crystallography is an experimental technique utilizing the fact that X-rays are diffracted by crystals (M. Wiener, 2008). Based on the diffraction pattern obtained from X-ray scattering off the periodic assembly of molecules or atoms in the crystal, the electron density can be reconstructed (M. Wiener, 2008). Since only intensities are measured, additional phase information, is required that is extracted either from the diffraction data or from supplementing diffraction experiments to complete the reconstruction. (This is referred to as the “phase problem” in crystallography). A model is then progressively built into the experimental electron density. The model is refined against the data, and the result is an accurate molecular structure.

1.2 Theory of X-ray diffraction

Scattering from an atom

The scattering from an atom is caused by the interaction of X-rays with electrons of the atom. The atomic form factor (f) can be expressed as the ratio of the amplitude of the scattering of the atom to the amplitude of the scattering from a single electron. The atomic form factor is given as

$$f = \sqrt{\sigma_e} \int_{V_{atom}} \rho(\vec{R}) e^{2\pi i \vec{H} \cdot \vec{R}} d\tau, \quad (1.1)$$

where \vec{R} is the coordinates of volume of elements, e is the electron, \vec{H} is the scattering vector, ρ is the electron density and $d\tau$ is $dx dy dz$.

Scattering from a molecule

In a molecule, all atoms scatter based on the atomic form factor (f). In general, the structure factor F of a molecule with N atoms is given as

$$F^M(\vec{H}) = \sum_{j=1}^N f_j e^{2\pi i \vec{H} \cdot \vec{R}_j}, \quad (1.2)$$

where N is the number of atoms in a molecule, f_j is the atomic form factor of j^{th} atom, \vec{R}_j is the position vector of j^{th} atom and \vec{H} is the scattering vector

Scattering from a crystal

A crystal is formed when molecules are arranged in a periodic lattice. The structure factor of a crystal with M atoms is given as

$$F^K(\vec{H}) = \sum_{m=1}^M f_m e^{2\pi i \vec{H} \cdot \vec{R}_m}, \quad (1.3)$$

where \vec{H} is the scattering vector, f_m is the atomic form factor of m^{th} atom, \vec{R}_m is the position vector of m^{th} atom, and M is the total number of atoms in the crystal.

Laue condition

Laue condition make the directionality of the process more obvious, as we have a set of three equations, one for each crystallographic axis that must be simultaneously satisfied.

The lattice factor (G) is given as

$$G = \sum_{u=0}^{U-1} e^{2\pi i \vec{H} \cdot u \cdot \vec{a}} \sum_{v=0}^{V-1} e^{2\pi i \vec{H} \cdot v \cdot \vec{b}} \sum_{w=0}^{W-1} e^{2\pi i \vec{H} \cdot w \cdot \vec{c}}, \quad (1.4)$$

where u , v and w are integer numbers.

The lattice factor (G) for the total unit cells is given as

$$G = U \cdot V \cdot W = N \quad (1.5)$$

where N is the total number of the unit cells.

The Laue-conditions are given as

$$\begin{aligned} \vec{H} \cdot \vec{a} &= h \\ \vec{H} \cdot \vec{b} &= k \\ \vec{H} \cdot \vec{c} &= l \end{aligned} \quad (1.6)$$

where h , k and l are integer numbers

Reciprocal lattice

A crystal consists of a periodic arrangement of unit cells in a lattice. A reciprocal lattice describes one in which the reflection parameters are directly related to real space parameters. If the unit of real space is measured in Å, dimension in reciprocal space can be written as Å⁻¹.

Ewald's sphere

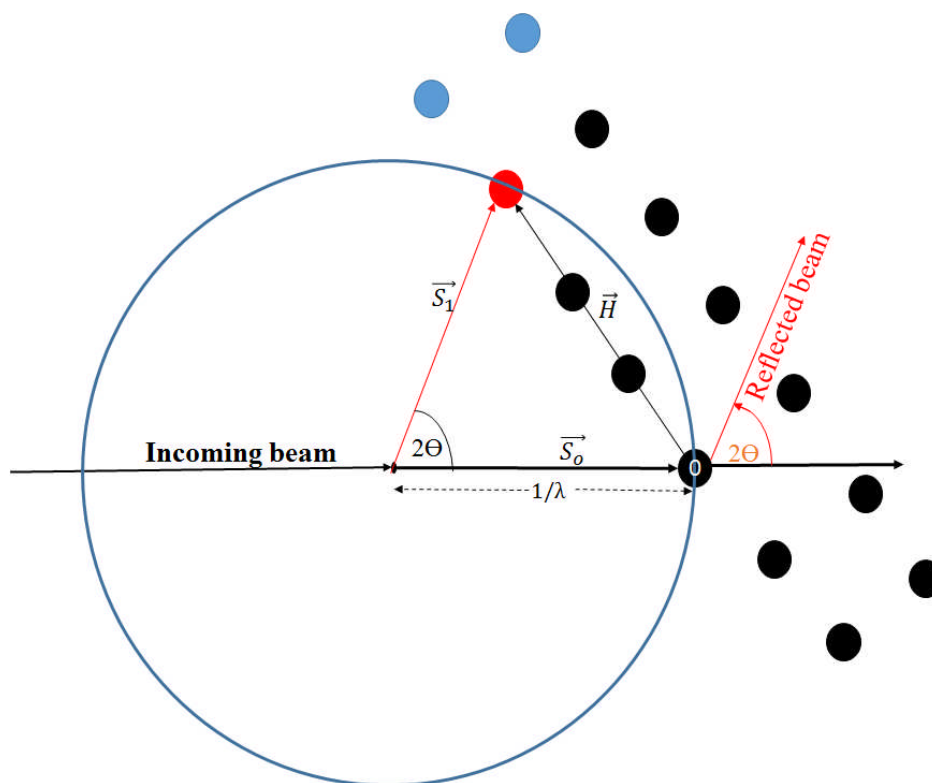


Figure 1-2: Ewald's sphere adapted from (N. Purwar, 2013). An Ewald sphere of radius $1/\lambda$ (\AA^{-1}), 2θ is the scattering angle, \vec{H} is the scattering vector. The directions of incoming and scattered beam are represented by \vec{S}_0 and \vec{S}_1 .

Ewald's sphere is a geometrical representation of wave vectors of the incoming and diffracted X-rays. The radius of the Ewald's sphere is inversely proportional to the wavelength of the employed radiation such as X-rays: For X-rays of larger wavelengths, the radius of the Ewald's sphere is smaller; on the other hand if the X-rays wavelengths are small, the corresponding Ewald's sphere is large in radius. Reciprocal lattice points that touch the surface of Ewald's sphere satisfy Bragg's Law and are in diffraction condition. The scattered beam passes from the crystal in the direction of the reciprocal lattice point.

The origin of the reciprocal lattice is at point O. Black dots, arranged in a periodic way denotes the reciprocal lattice points. The directions of incoming and scattered beam are represented by \vec{s}_0 and \vec{s}_1 . The length of vectors \vec{s}_0 and \vec{s}_1 are the same due to the elastic scattering condition.

Bragg's Law is given as

$$\sin \theta = \frac{2}{\frac{|\vec{H}|}{\lambda}}, \quad \frac{\sin \theta}{\lambda} = \frac{1}{2d}, \quad (1.7)$$

where d is the distance between atomic layers in a crystal, λ is the wavelength of the incident X-ray beam, \vec{H} is the scattering vector and 2θ is the scattering angle.

1.3 Biological background

1.3.1 Photoactive Yellow Protein (PYP)

Historical perspective

The presence of PYP a brightly yellow colored soluble protein, was discovered during the isolation and characterization of several photosynthetic electron transfer proteins (cytochromes, iron-sulfur proteins) from Ectohiorhodospira halophile (Meyer, 1985) bacterium. Ectohiorhodospira halophila (Meyer, 1985) lives in sunny place, hypersaline lakes, shown in the figure 1.4 (a) and is the most halophilic bacterium known (Imhoff *et al*, 1978). Ectothiorhodospiraceae (Imhoff, 1984) are phototrophic sulfur bacteria which deposit elemental sulfur outside the cells during oxidation of sulfide and are considered anomalous members of the family Chromatiaceae.

All species of *Ectohiorhodospira halophila* are motile by using a polar flagella. There are other type strains of this organism from the natural environment (Imhoff *et al*, 1978; Imhoff 1984; Stackebrandt *et al*, 1984; Ivanova *et al*, 1985). The organism is a strict anaerobe and can live in temperatures up to 50°C. Its optimal growth conditions are 11-22% NaCl, and it can survive in up to 32% salt. Its alkaline optimal growth conditions range from pH 8.8-9.0, but it also tolerates a pH of up to 11(Grant & Tindall 1986;1990).

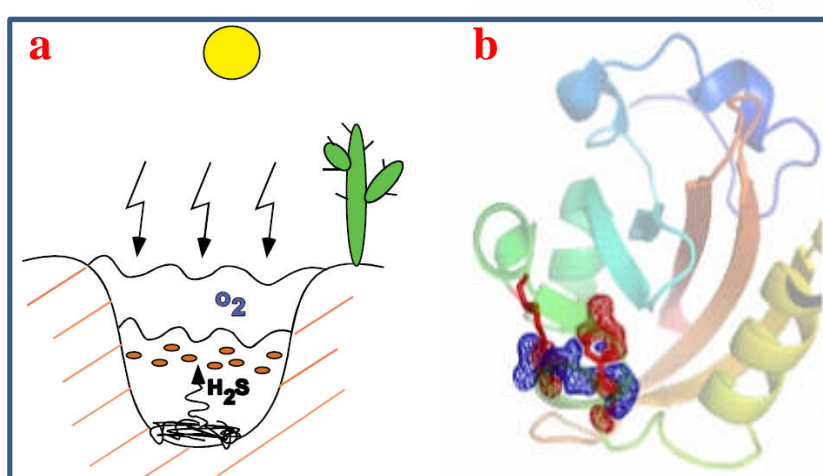


Figure 1-3: PYP from Dr.Schmidt's lecture notes :(a) *Ectohiorhodospira halophila*, which lives in sunny, hypersaline lakes (b) Ribbon structure of Photoactive yellow protein (PYP).

Properties of PYP

PYP is a soluble cytosolic protein with a molecular mass of 14kD (Meyer *et al*, 1987). The visible wavelength peak (446nm) of the pure protein is more than twice as intense as the (276 nm) protein peak. Upon laser excitation, the protein shows photo activity (Meyer *et al*, 1987), and it has a photocycle similar to the membrane protein bacteriorhodopsin. PYP has been isolated from other type strains of the phototrophic bacteria (Meyer *et al*, 1990, 1993) and identified immunologically in many other bacteria (Hoff *et al*, 1994b).

1.3.2 Cytochrome c nitrite reductase (ccNiR)

Cytochrome c nitrite reductase (ccNiR) is a central enzyme of the nitrogen cycle. It binds nitrite and reduces it to ammonia by transferring six electrons. This ammonia can then be utilized to synthesize nitrogen containing molecules such as amino acids or nucleic acids. (M.D. Youngblut, 2013).

Schewanella oneidensis is a gram negative γ -proteobacterium originally isolated from Lake Oneida, NY in 1988. The organism uses oxygen as the final acceptor of these electrons, in which case water is formed (M.D. Youngblut, 2013). However, some of these bacteria can use alternative electron acceptors such as nitrite, which is where ccNiR comes in. This organism is unique in that it can respire using over two dozen different terminal electron acceptors, which include inorganic compounds such as nitrate and nitrite, organic molecules such as formate and dimethyl sulfoxide, and even metals such as manganese(V) and uranium(VI) (M.D. Youngblut, 2013). The c-heme proteins are often highly efficient in electrons transfer functions, and it has been hypothesized that *Schewanella oneidensis* has a variety of respiratory options due to the presence of the large number of these proteins (M.D. Youngblut, 2013). Among the c-heme proteins encoded by *Schewanella oneidensis* is ccNiR, which catalyzes the reduction of nitrite to ammonia.

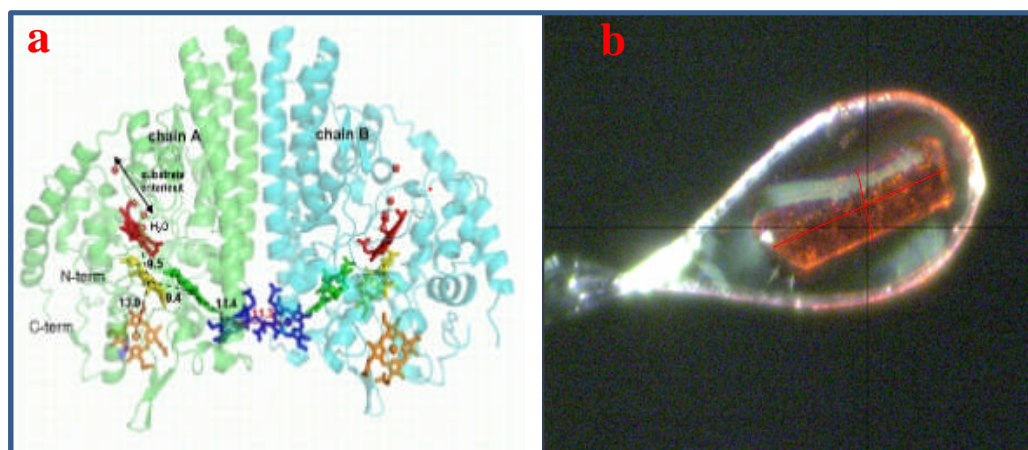


Figure 1-4: (a) ccNiR adapted from Matthew Youngblut, Evan T. Jud, and A. Andrew Pacheco, 2012 (ribbon representation)(b) Cytochrome c nitrite reductase (ccNiR) crystal mounted using a cryoloop with width of 250mm and length of 400mm.

1.4 Overview of the X-ray crystallographic method

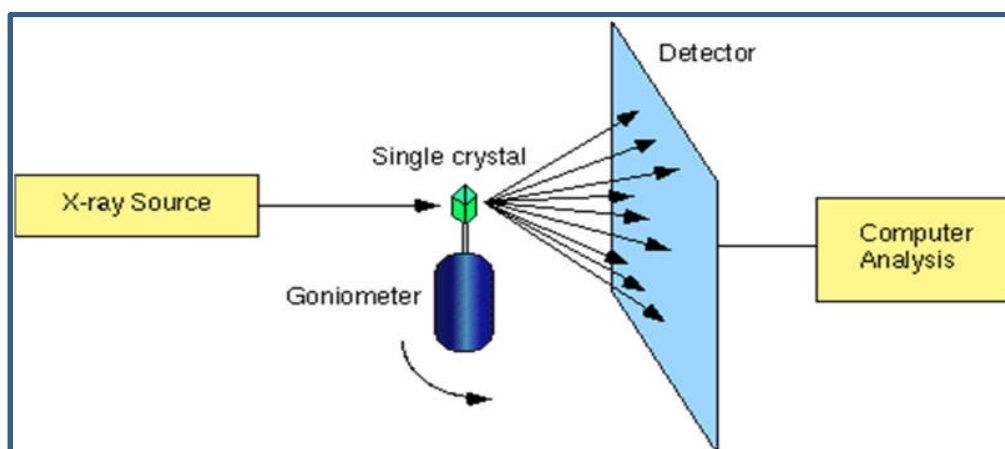


Figure 1-5: A bird's eye view of an X-ray experiment. The X-ray beam is produced by the source on the left hitting the crystal mounted on the goniometer. Scattered X-rays (diffracted and background) are detected on the charge coupled device (CCD) detector.

A simple representation of the X-ray experiment is shown in figure 1.5. The goal was to obtain the electron density of crystal PYP or ccNiR which was used for the study. The X-

ray beam is produced by the source (X-ray) hitting the crystal mounted on the goniometer. The X-ray diffraction pattern was recorded by a detector. The data collected from the detector was analyzed using Imosflm, CCP4 and COOT software used to obtain the electron density.

1.5 My contribution

I contributed to the construction of a LMXS-PC. I also contributed my work to a Stepper Motor Controller (SMC), which is used for moving the MarCCD detector, as well as for crystal rotation. A user interface was built to control the SMC which explained in Section 2.3.3. This effort improved the efficiency of aligning the crystal in the goniometer with automated user interface (using C#, TCP/IP protocol). I was also involved in the development of a program designed to transparently overlay on the camera a digital image; this enables users to take quick measurements of the protein crystal size using a mouse, which is explained in Section 2.3.5. I prepared two types of buffer solution for protein crystallization, which is explained in Section 2.4.1 and Appendix IV. Finally, I collected the data by mounting the crystal which is described in Sections 2.6.1 and 2.6.2. The diffraction pattern for PYP and ccNiR is detailed in Sections 4.1 and 4.2. The goal was to obtain the electron density map, which explained in Sections 4.4.1 and 4.4.2, and data statistics results are described in Section 4.3.

Chapter 2

Materials and Methods

2 Introduction

In Chapter 2, I provide an overview of the design of the micro focus X-ray source done in Prof. Schmidt's Laboratory Microfocus X-ray Source for Protein Crystallography (LMXS-PC) facility. The detailed explanation of each hardware component is given below in section 2.2. The software that controls the hardware components is also explained in section 2.3. After assembling it, the instrument was tested by conducting a crystallographic study of a known crystal. The method of growing protein crystal is explained in the section 2.4. The mounting of crystals by different techniques is explained in section 2.5. The data is collected at different temperatures and by different mounting techniques to determine the quality of the instruments.

2.1 Setup of a self-designed micro-focus X-ray source

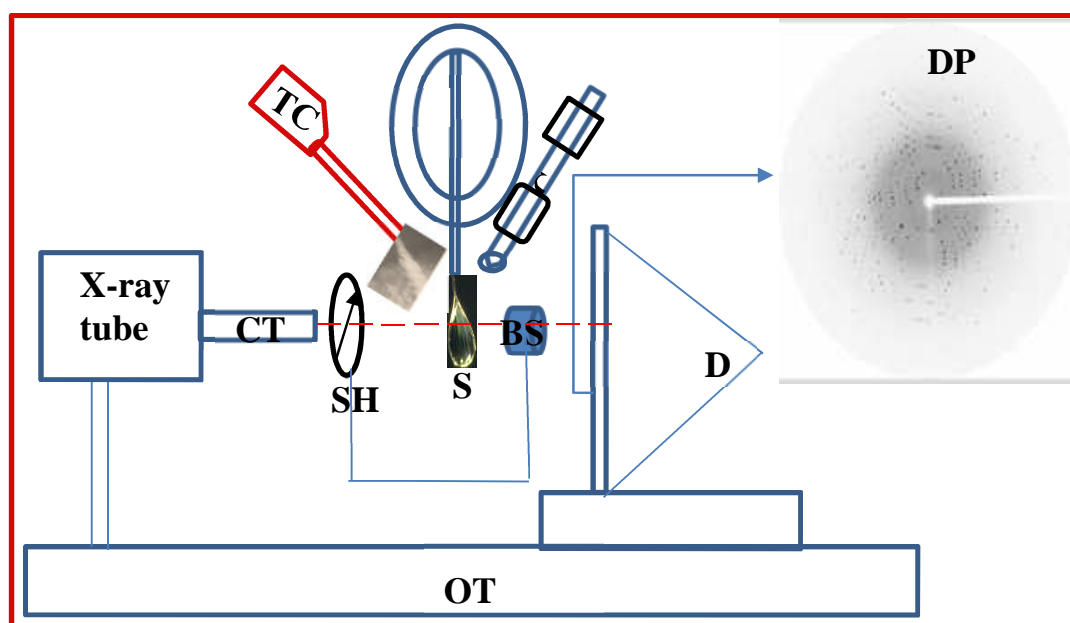


Figure 2-1: Components of microfocus X-ray source : CT-Collimator Tube, BS-Beam Stop, SH-Shutter, TC-Temperature Control, G-Goniometer, C-Camera, S-Sample, D-Detector, OT- Optical Table, DP-Diffraction Pattern.

The laboratory X-ray sources can be classified into two types: sealed-tube and rotating anode. Both may be used to generate monochromatic X-ray radiation. Rotating anode generators (W. Longley) are expensive (approximately \$450,000, from rigaku manual) and require high maintenance, but are the most powerful laboratory X-ray source available.

The sealed-tube X-ray source, which are small and is less expensive (approximately \$94,800, from Genix manual). It can be used to initially scan for crystals. The Schmidt laboratory has built a micro focus X-ray source for protein crystals. Figure 2.1 shows the setup of the self-design micro focus X-ray source built in the M.Schmidt's laboratory. The details of each hardware component are explained in Section 2.2.

2.2 Hardware components of the X-ray source

Mirror

The Xencos Fox optics are based on the principle of diffraction. In the Xencos mirror, a multilayer coating assures constructive interference of the reflected rays based on Bragg's Law. The multilayer coating is used mainly as a narrow band pass filter.

2.2.1 Genix head

The Genix beam delivery system is based on a compact, water-cooled, micro-focus X-ray source (Genix manual). The resulting combination runs at 50 watts. The X-ray source is very stable, requires little maintenance, and has a reduced operational cost. The optics combine to allow Genix to deliver an intense X-ray beam as shown in Figure 2.2(a).

2.2.2 The control unit

The control unit is user friendly and has a touch screen interface. It enables the user to control key parameters such as automatic power ramp-up, monitoring of source stability, and automatic shutdown (Genix manual). The control unit of the Genix is shown in Figure 2.2(b). The system is designed to maintain an extended X-ray tube lifetime and to adapt to the user mode of operation in local or remote control.

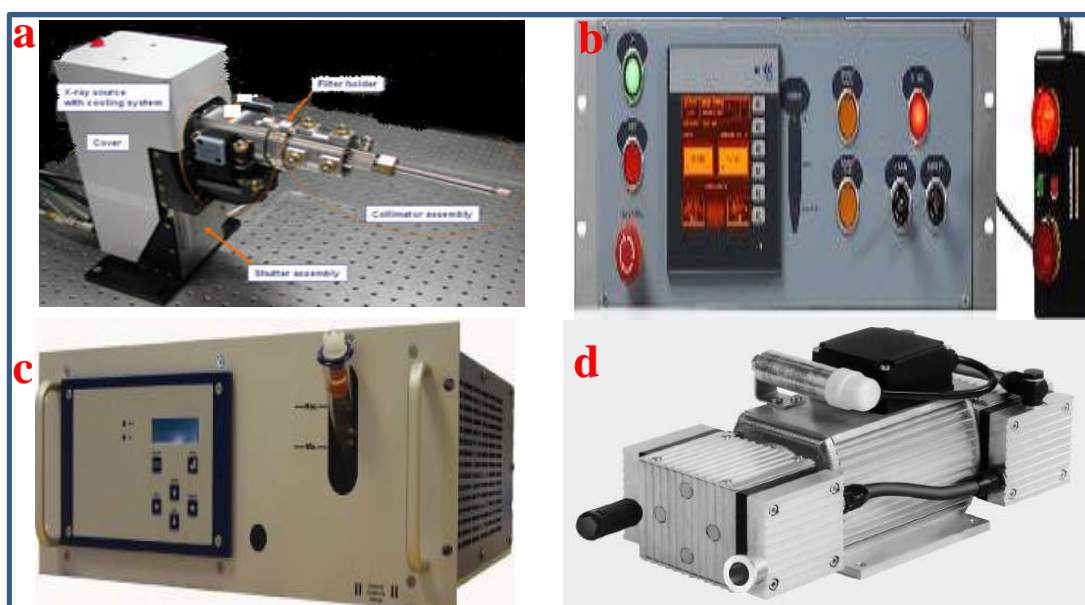


Figure 2-2 : (a) Genix beam delivery system (b) The control unit (c) Water to air chiller (d) Vacuum pump (from the Genix manual).

2.2.3 Water-to-air chiller

The water-to-air chiller is a compact, closed loop cooling device which guarantees thermostabilization of the Genix X-ray generator (Genix manual). Figure 2.2 (c) shows the front view of the water-to-air chiller. The purpose of the chiller was to cool the X-ray source.

2.2.4 Vacuum pump

The gas-tight vacuum pump was used in the experiment evacuation of air and gases and is capable of providing a 100% oil-free operation (Genix manual). Figure 2.2 (d) shows the entire view of the vacuum pump. The vacuum pump has a white tube which connects it to the Genix head; it used mainly to protect the inside of Genix head.

2.2.5 AVT camera

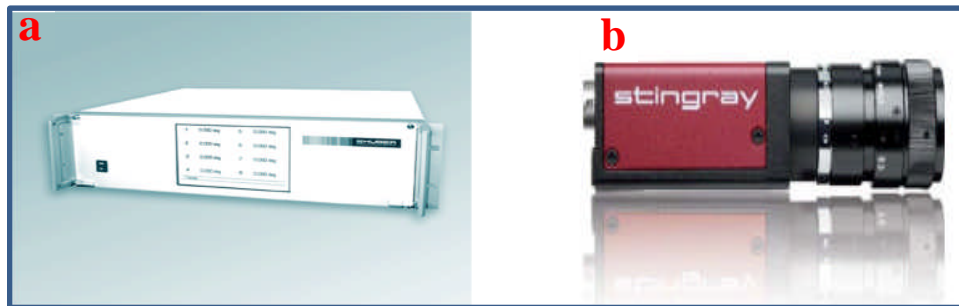


Figure 2-3: (a) SMC 9300 Motor controller (from the manual of the SMC controller) (b) Sideview of the AVT camera (alliedvisiontec manual).

The stingray camera from Allied Vision Technologies (AVT) is a versatile, powerful camera for many applications, and an ideal custom camera (alliedvisiontec manual). It boasts an excellent image quality and incorporates an advanced set of camera features.

Stingray cameras are available with daisy chain FireWire connectors or with both copper and glass optical fiber (GOF) ports (alliedvisiontec manual). Figure 2.3(b) shows the side view of the AVT camera.

2.2.6 SMC 9300 controller

The motor controller Stepped Motor Controller (SMC) 9300 is an intelligent control system which supports up to 16 step motor axes, which can be simultaneously and independently operated. Its flexible and modular design enables the user to easily adapt the instrument (SMC manual). Figure 2.3(a) is the front view of the SMC 9300 from the SMC manual. Manual operation and configuration of the unit is done via touch screen display. The controller is able to accommodate special configurations and versions, as well as customer-specific adaptations and individual control software requirements (SMC manual).

2.2.7 Cryojet

The cryojet was designed to operate in an X-ray diffractometer.

Sample flow unit

The rigid tube of sample flow is immersed in the liquid nitrogen in the storage dewar. By the time it boils the nitrogen, cold gas passes up to the flexible stainless steel vacuum-insulated transfer tube and into the cold head, as shown in Figure 2.4(a). The cold head has a heat exchanger, a heater and a temperature sensor just inside the nozzle (cryojet manual). Next, the gas goes through the nozzle and the sample flow is obtained. The temperature of the sample flow ranges from between $90^{\circ} - 300^{\circ}\text{k}$.

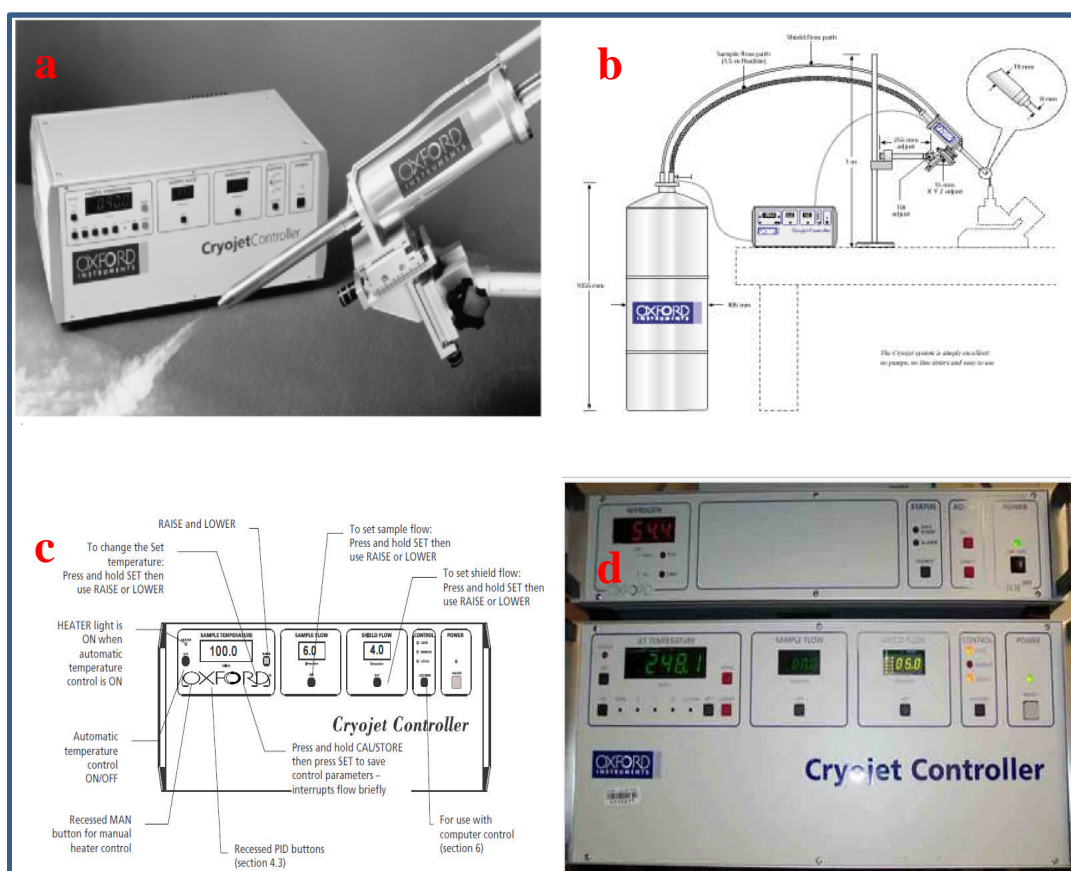


Figure 2-4: (a) The view from the top of the control unit and dewar head (from the cryojet manual), (b) Overall view of cryojet system (c) Cryojet controller front panel (from the cryojet manual) (d) Cryojet controller full details front panel (photograph from Prof.Schmidt's laboratory).

Shield flow unit

The rigid tube of the shield flow is the same as the sample flow unit; it is also immersed in the liquid nitrogen in the storage dewar. The top of the unit are the heat exchanger, heater and a temperature sensor, which heat the nitrogen (for the room temperature). At this point, the nitrogen is ready to flow through the central stub of the shield unit to the cold head using polythene tubing (cryojet manual).

2.2.7.1 Front panel operation

The front panel (figure 2.4(c)) operations of the cryojet controller are listed below:

Power ON/OFF

When the user turns on the instrument, it looks for the type of interface is used in the experiment. The ISOBUS address is used for the serial interference. Figure 2.4(d) shows the cryojet controller of the front panel.

LOC/REM control

The cryojet can be used either by local or remote control. The remote control is used for monitoring it remotely on a computer (cryojet manual). When it is not connected remotely with the computer, the user can operate it manually. If it is connected remotely, the raise/lower button cannot operate.

Flow displays and SET button

The liquid nitrogen gas flow to the shield and sample flow is measured in liters/min. The flow can be set based on user's need. By holding the SET button, the user can raise or lower the flow level according to his need in the experiment.

Sample temperature control

In the cryojet controller, the temperatures are displayed in Kelvin. By pressing the set button, the temperature can be set based on the user's requirements; By holding it, the temperature can be changed using the raise/lower button. Once the required temperature is

set in the controller, the user can set the sample flow and shield flow based his needs. After the flow is set, the heater is turned on. The heater must be on when the nitrogen is flowing to prevent the accumulation of ice in the bottom of the nitrogen dewar.

2.2.8 MarCCD 165 detector



Figure 2-5: Shows as the complete view of the MarCCD 165 detector.

X-ray conversion to light by phosphor screen

X-rays passing through the front window of the detector are absorbed by a phosphor screen, which then converts them into visible light (MarCCD manual). A phosphor is used because a CCD sensor has peak quantum efficiency in the visible region and very low quantum efficiency for detecting X-rays directly, and because the maximum sizes of CCD chips are too small (MarCCD manual). Then, a large area of light from the phosphor screen is demagnified by a fiber optic taper onto the CCD sensor. Figure 2.5 shows the complete view of the MarCCD 165 detector.

Integrating detector

A CCD detector is an integrating detector, as opposed to a counting detector. This means that individual X-rays on the detector are not distinguished as they strike; rather, the detector begins in a cleared state and then integrates the incident signal for a specified amount of time, and finally reads out the total signal accumulated in each pixel (MarCCD manual). Counting detectors count each photon as it strikes and can have advantages at the lowest signal levels (MarCCD manual).

Analog to digital conversion and data path

During the data readout for each pixel, an analog voltage is received from the readout channel on the CCD (MarCCD manual). On each channel, this signal passes through an amplifier, is modified by an analog offset to match the A/D converter input, and then is converted to a digital signal by an A/D converter (MarCCD manual).

Background subtraction and image correction

The corrected images are achieved by three major steps: background subtraction, spatial correction and flat field correction (MarCCD manual).

The background subtraction is done for two important reasons: i) The voltage level that corresponds to zero signals is different for each channel and ii) The bias voltage in the electronics may drift over time. The software, by default needs to have the background image already collected and stored in the background buffer before starting to collect the data images (MarCCD manual). The default program reads the bias level of the detector

twice and produces a dezingered (MarCCD Manual) background. The background must be periodically recollected in case of any drift in the bias levels.

The cold operating temperature and resulting low, dark current which the user saves the background image is a very important, time-consuming step.

Cooling system

The cooling system is important in the detector because the CCD sensor needs to be cooled to reduce the dark current (MarCCD manual). The CCD sensor temperature must be at -70°C or below; the detector should not run at a warmer temperature. If the temperature is below -120°C, it can affect the imaging performance and also damages some components due to stress. The cooling system of the CCD sensor operates as a closed-cycle refrigeration system.

2.2.9 Fast shutter



Figure 2-6: (a) Shutter controller(sc10) (b) SH05(shutter) (from Thorlabs).

The Shutter controller(SC10) model is a type of digital shutter control which is designed to control the shutter (SH05) shown in Figure 2.6(b). The SC10 shown in Figure 2.6(a) features three user interfaces: a manual front panel, control from a personal computer (PC) and control from a TTL (Transistor-Transistor logic) direct interface (Thorlab shutter manual).

The purpose of the front panel is mainly for the user to control the shutter condition (open/close); but it is also useful for its auto, single shot and repeated modes.

The shutter SC10 can also be controlled from the PC using a RS-232 interface. This saves the user work and provides a remote control option. The TTL interface is more complex compared to the other two methods of interface.

The fast shutter plays an important role in the experiment. The MarCCD program command is sent when the shutter must be in the open or close condition. When the X-ray shutter is opened, it in turn opens the fast shutter, and the beam passes through it and hits the detector. After collecting the required data, the shutter closes and stays idle. The shutter- operates based on the time the user wants to open or close it.

2.2.10 Optical table



Figure 2-7: Optical table (from Thorlabs).

The optical table is the standard table for vibration control. It meets all requirements for structural stiffness and damping and is recommended for the majority of optical table applications, from pulsed laser experiments to holography and interferometry (Optical table manual). Figure 2.7 shows the optical table where the entire instrument is mounted on top of the table. It has the highest core-density and smallest honeycomb cell area. Individual nylon cups under each drilled and tapped mounting hole are airtight, making the top spill-proof (Optical table manual). For more optical table vibration-sensitive work or noisy environments, a active vibration cancellation system may be required (Optical table manual). The hardware components that are controlled using software are mentioned in Chapter 2.3.

2.3 Software used to control hardware components

2.3.1 Software for X-ray control unit



Figure 2-8: Genix utility software (screen shot).

The Genix software connects the (Genix) control unit and the computer provides the ability to control the unit remotely so that the users do not need to be in the X-ray unit area. The software uses Transmission Control Protocol (TCP)/ Internet Protocol (IP) for communication. The commands are transmitted using hexadecimal code. This control unit also has the ability to operate in manual mode, use of the manual method have to be physically present to control the unit. The remote mode offers the flexibility and ability to control the unit remotely from any computer connected to the Local area network (LAN) or the Internet through a virtual private network (VPN) tunnel. Figure 2.8 shows the outline of Genix utility software.

The software gives users the ability to check the mode, chiller temperature and power stability and to set voltage, current and shutter speed.

2.3.2 Software for the SMC controller

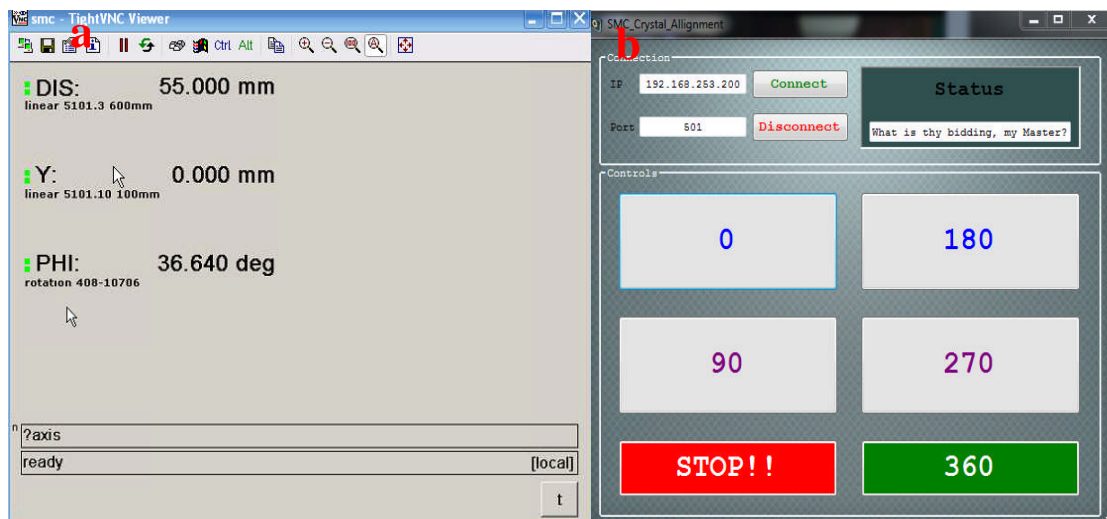


Figure 2-9: (a) SMC software (b) SMC crystal alignment tool (screen shot).

The SMC controller software allows users to connect to the SMC unit using tight VNC (Virtual Network Computing) viewer with TCP/IP protocol. The tight VNC viewer acts like a remote control for the system. Figure 2.9(a) shows the display details completely, including the distance (dis) of the detector from the center of camera and the goniometer. The Phi axis shows the position of the goniometer where the crystal is mounted in the system.

2.3.3 SMC crystal alignment tools

The SMC crystal alignment software was designed and developed as part of this thesis using C# and on the foundation of TCP/IP protocol. The above user interface is connected to the instrument using the IP address and port configuration from the client's side. The status bar shows the connection status. Figure 2.9(b) shows the display view of the crystal alignment software tool, which was used in the data collection process for this project. The orientation of the goniometer is controlled by the user based on his requirements. The various control buttons are used to rotate the goniometer to particular angles. Once the crystal is mounted in the goniometer, the DEGREE button controls the rotation around the Phi axis and the STOP button stops the rotation of goniometer at particular points needed.

2.3.4 Software for MarCCD

MarCCD GUI used to set the initial setup

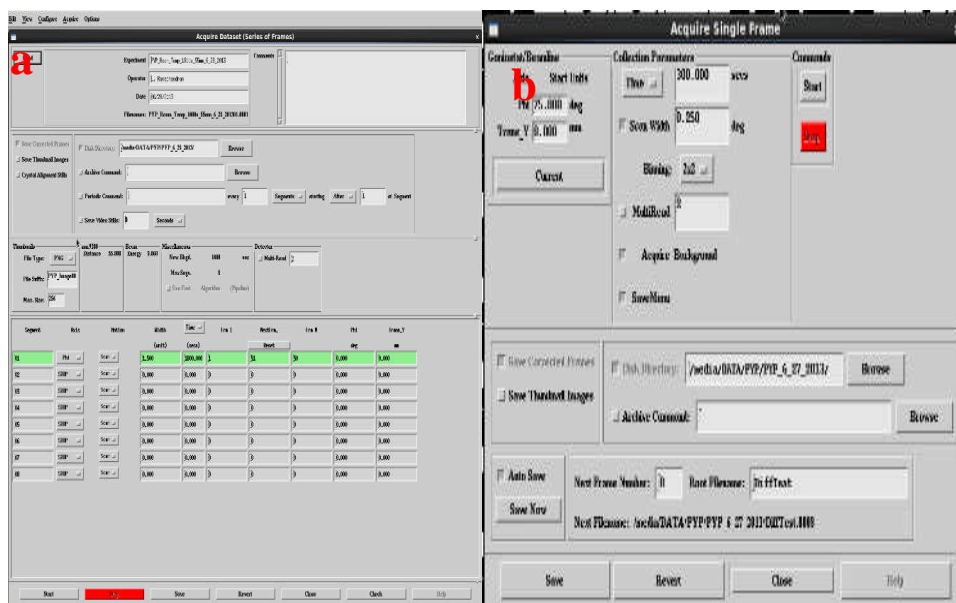


Figure 2-10: (a) MarCCD graphical user interface used to initial setup (b) MarCCD GUI that is used to collect single frame data (screen shot).

The initial setup done by the user based on the requirements needed to collect the data set: time, width and number of frames. The filename must first be saved in the folder correctly. Then the user chooses “axes” and picks “PHI” and save the axis as “PHI”. The user sets time and width according to his particular experiment. The PHI (degree) can also be set based on the user’s needs for the crystal rotation in the goniometer. The user can set the number of frames to collect the data set in the experiment and save the configuration. Finally, the user clicks the “start” button to collect the data and save the data in the required folder. The GUI that was used for the initial setup in MarCCD is shown in Figure 2.10(a). The GUI shown in Figure 2.10(b) is used to collect the data for a single frame set.

GUI used to collect data

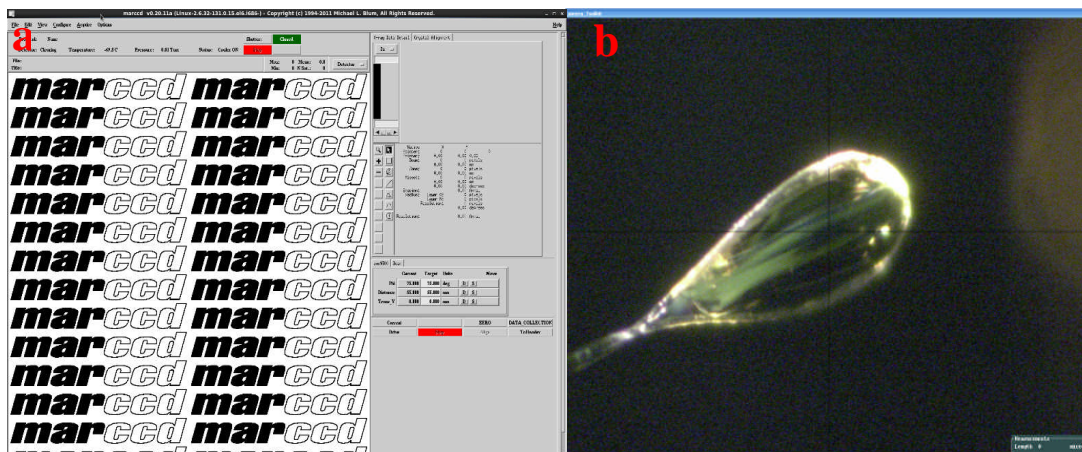


Figure 2-11: (a) GUI that is used to collect the complete data set, (b)Crystal Toolkit software (screen shot).

The GUI shown in Figure 2.11(a) is used to collect a complete data set. All information is entered in the system manually before starting to collect data, as explained in section 2.10. The GUI in Figure 2.11(a) displays the distance of the detector and the rotation of the goniometer axis during data collection. The diffraction pattern is shown in the center of the screen, where the user can check the resolution of the data. The top middle section displays the temperature of the cooling system. The cooling system, the importance of which is explained in detail in Section 2.2.8, has to be monitored constantly during the data collection process.

2.3.5 AVT camera software

The AVT camera software is used by crystallographers to measure both the length and the width of a crystal. Figure 2.11(b) shows the GUI used for crystal measurement. This program helps to get an accurate crystal size, but it can also monitor crystal rotation.

2.4 Protein crystallization

2.4.1 Preparation of buffer solutions

Two types of buffer solutions were prepared in the protein crystallization trials: One of the buffer solutions is 3.0M of Ammonium Sulphate, 300mg/ml of sugar or sucrose, 15% of glycerol and 50mmol of $\text{Na}_2\text{H}_2\text{PO}_4$ (monobasic monohydrate) plus water for total volume of 50ml. Another buffer solutions is 3.2M of Ammonium Sulphate, 300mg/ml of sugar or sucrose, 15% of glycerol and 50mmol of $\text{Na}_2\text{H}_2\text{PO}_4$ (monobasic monohydrate) in water a total volume of 50ml.

The detailed procedure of preparing cryobuffer is described in the Appendix 7 Section 4. After the buffer stock solutions were prepared, they were filtered through 0.22 μm sterile Millex filters prior to use. The desired pH values of all the buffers mentioned above were adjusted by adding 10 M NaOH prior to bringing solutions to 50 ml.

2.4.2 Crystallization methods

There are at least seven practical methods used for macromolecular crystallization. These include vapor diffusion, bulk crystallization, batch, free-interface diffusion, dialysis, temperature-induced, and seeding (K. Geethanandan, 2011). Among these methods, vapor diffusion and microbatch (a newly developed method from an old technique) are the most

popular means being utilized by crystallographers to obtain macromolecular crystals (K. Geethanandan, 2011). The most common protocols are the hanging drop and sitting drop methods (S. McPherson, 1998).

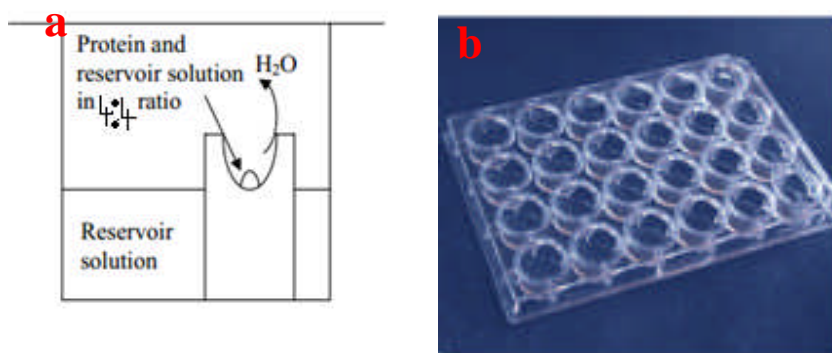


Figure 2-12: (a) The sitting-drop vapor diffusion method for protein crystallization (b) Crystallization plate (picture from Hampton research).

PYP crystals are grown using the sitting drop vapor diffusion method, which is performed using a 24 well depression plate. 4 μL of protein solution and 4 μL of reservoir solution are mixed together at the top of a ledge, as shown in Figure 2.12(a). The basic principle of this method is straightforward: A drop composed of a mixture of macromolecule sample and precipitating solution is placed in vapor equilibrium with a reservoir solution of precipitant and buffer (K. Geethanandan, 2011). The crystallization plate is shown in Figure 2.12(b).

2.5 Methods for mounting crystal

2.5.1 Cryoloop

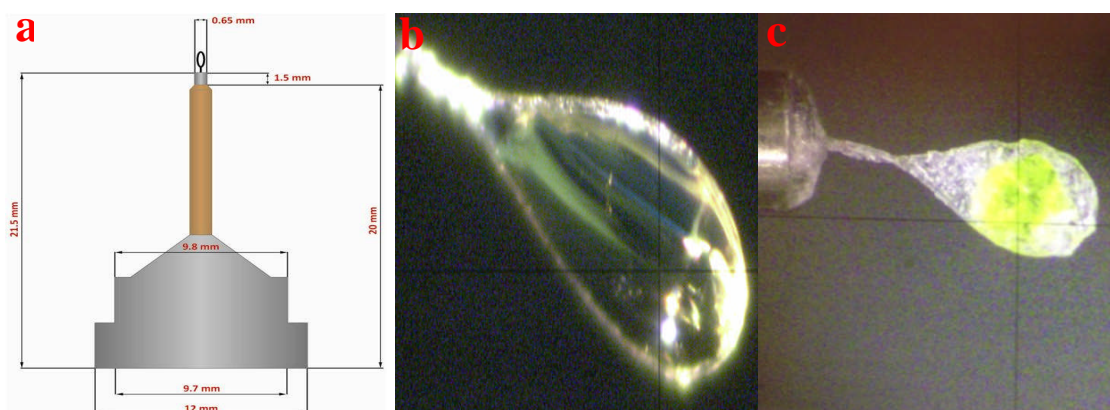


Figure 2-13: (a) Cryoloop properly installed in a magnetic mounting base (picture from the Hampton Research) (b) Crystal perfectly frozen using cryoloop (c) Crystal imperfectly frozen (screen shot).

Crystal mounting for PYP can be carried out using capillary tubes, fine glass capillary tubes, thin glass spatulas, or thin loop films; however, the loop mounting technique has become the prevalent procedure for crystal mounting at cryogenic temperatures (Rodgers, 1997). Originally, (K. Geethanandan, 2011) the loops were made from copper or tungsten wire with 1-2 mm diameters and 25-75 μm thickness, but now they are made from fine nylon fibers with 0.05-1.0 mm diameters and 10 and 20 μm thickness. Figure 2.13(a) is a picture of a cryoloop properly installed in a magnetic mounting base from the Hampton Research.

It is best to select a loop that is just wide enough to keep the crystal from dropping off (K. Geethanandan, 2011). For instant data collection, the crystal is picked up and immediately

mounted in the goniometer. Before mounting the crystal, the sample flow, shield flow and temperature are set in the cryojet controller. Figure 2.13(b) shows crystal that has been perfectly frozen while (c) shows as a poorly timed frozen crystal.

The other advantage of the cryoloop method is that crystals that are diffracted well can be kept and sent to a synchrotron after screening at LMXS-PC facility. In principle, once the crystals have been successfully cooled to cryogenic temperatures, they can be kept for an indefinite time (Parkin and Hope, 1998).

2.5.2 Mitegen loop

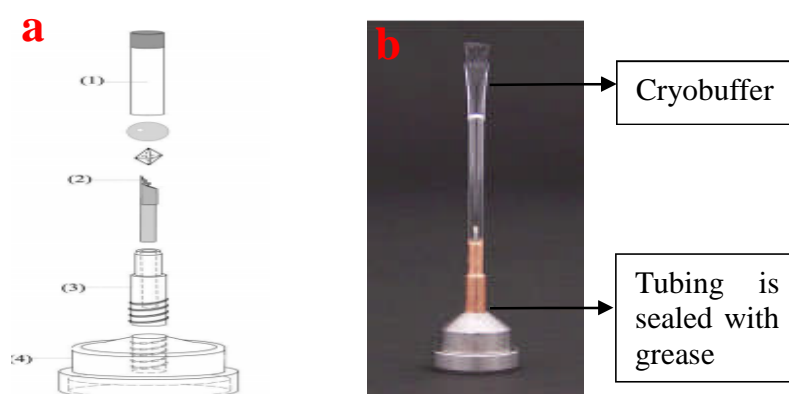


Figure 2-14: (a) Schematic diagram of a room-temperature loop mounting technique (b) Photograph of the room-temperature mount (from Hampton Research).

Figure 2.14(a) shows the design of room-temperature mounts. They consist of (1) a short piece of thin-wall (12.5-50 mm) optically transparent tubing with a fixed crystal-size-independent diameter of roughly 2 mm; (2) a micro fabricated crystal holder precisely attached to a solid stainless-steel rod, (as described in Thorne *et al*, 2003); and (3, 4) a magnetic stainless steel goniometer-compatible base that captures the rod and seals with the tubing (Y. Kalinin, 2005). To prepare a sample for X-ray data collection, the stainless

steel rod attached to the micro fabricated (Y. Kalinin, 2005) crystal holder mount (2) is inserted into the goniometer-compatible base (3, 4) and held in place using grease. A plug of stabilizing (cryobuffer) solution used to maintain a humid environment during storage (Y. Kalinin, 2005) and data collection is injected using a syringe needle as close to the sealed end of the tubing as possible, as shown in figure 2.14(b). Next, a crystal is retrieved from the well using a micro fabricated crystal holder and excess liquid is removed (as discussed by Thorne *et al*, 2003). Finally, the tubing (whose inside diameter of 2 mm is roughly three times the outer dimensions of the mount and rod) is pushed over the mount and onto the base with which it forms an airtight seal (Y. Kalinin, 2005). A small amount of grease applied to the base can be used to ensure the integrity of the seal.

2.5.3 Capillary mount

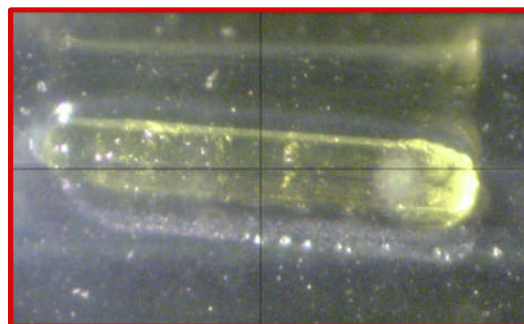


Figure 2-15: PYP crystal is inside the quartz glass capillary tube (screen shot).

Crystal clear quartz capillaries are thin walled (approximately 10 micron wall thickness). The length of the capillary has a well-defined diameter, with one end having a funnel shape and the other end closed (hampton research). Quartz capillaries have a wall thickness of 0.01 mm and an overall length of 80 mm +/-5 mm. They are available in a wide range of outside diameters from 0.1 mm to 5.0 mm (hampton research). They are designed to mount,

hold, and store small molecules and biological macromolecular crystals for X-ray data collection (hampton research). Capillaries can also be used for crystal density measurements and crystal growth experiments and can be sealed tightly against moisture using epoxy glue. Figure 2.15 shows the PYP crystal inside the capillary tube during the data collection.

For 0.1 mm to 2.5 mm capillaries, the open end capillary tube base size is 3.0 +/- 0.2 mm OD x 0.2 +/- 0.15 mm wall thickness; for 3.0 and 3.5 mm capillaries, the open end capillary base size is about 4.4 mm OD x 0.25 mm wall thickness (hampton research). For 4.0 and 5.0 mm capillaries, the open end capillary base size is about 6.0 x 0.25 mm.

2.6 Data collection

2.6.1 PYP crystals mounted in a cryoloop



Figure 2-16: (a) Perfectly frozen crystal the length is 580mm (b) Perfectly frozen crystal the width is 185mm (screen shot).

The data collection is done to test the performance of the instrument. In this case, the data is collected at cryogenic temperature (100°k). The most important factor required for

evaluating data quality is the completeness of the X-ray data, including all the indices and their associated intensities, with their standard uncertainties (Dauter, 1999). The factors that influence the data completeness are the geometric factor. The geometric factor, arising from the symmetry of the crystal lattice and the detector setup, is a quantitative factor related to a number of variables, the selection of the total rotation range appropriate for the crystal symmetry, the crystal-to-detector distance, crystal mosaicity and beam divergence (N. Chandra, 2013). Quality of the data is the range of the detector reflected by R-factor. The longer the exposure time, the greater the intensities and the signal-to-noise ratio, and the better the data quality obtained (Dauter, 1997; Dauter, 1999).

The X-ray data quality for macromolecular crystallography is assessed by a global indicator, the merging R-factor (R_{merge}). The merging R-factor is defined by the following equation (Blundell and Johnson, 1976):

$$R_{merge}(I) = \frac{\sum_{hkl} \sum_i |I_i(hkl) - \langle I(hkl) \rangle|}{\sum_{hkl} \sum_i I_i(hkl)} \quad (1.8)$$

where, \sum_{hkl} is the multiple measurement and symmetric equivalent reflection, I_i is the intensity of the measured reflection and $\langle I \rangle$ is the average intensity from multiple reflection. Figure 2.16(a) and (b) show as the length and width of the crystal.

The R_{merge} value will be between 5-10% while the signal/noise ($I/\sigma(I)$) falls around 1.0–2.0% (Dauter, 1999) in the highest resolution shell. The value of the merging R-factor is almost universally used for evaluating X-ray diffraction data (N. Chandra, 2013). The room temperature data set is collected for comparison with the low temperature data set.

2.6.2 PYP crystals mounted in a mitogen loop

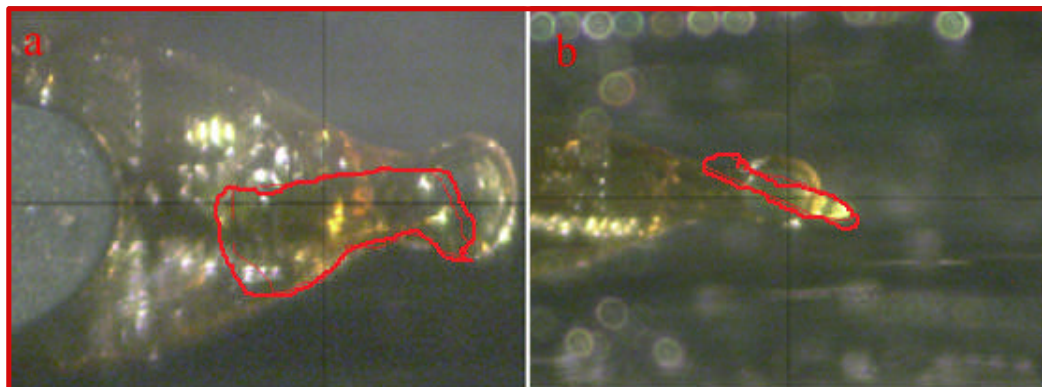


Figure 2-17: (a) Crystal mounted by mitogen loop with length of 390 mm and width of 105 mm (b) Crystal mounted by mitogen loop show side view (screen shot).

With this data collection method, X-ray data can be collected at room temperature (273k).

In this method, the PYP crystal is mounted using a mitogen loop in a plastic sleeve. Figure 2.17(a) Crystal mounted by mitogen loop with length of 390 mm and width of 105 mm and Figure 2.17 (b) show the side view.

The R_{merge} (described in Section 2.6.1) value will be between 5-10% while the signal/noise ($I/\sigma(I)$) falls around 1.0-2.0% (Dauter, 1999) at highest resolution shell. The quantity of merging R-factor is almost universally used for evaluating X-ray diffraction data. The R-factor is 4.2.

Chapter 3

Software for Electron Density

3. Data reduction and analysis

3.1 Introduction

Chapter 3 describes a scheme to reduce a data sets. The first step is obtaining a crystal. The diffraction patterns are collected using the micro focus X-ray. Diffraction patterns for the same crystal are collected. The goal is to obtain the electron density map and interpret it with an atomic model.

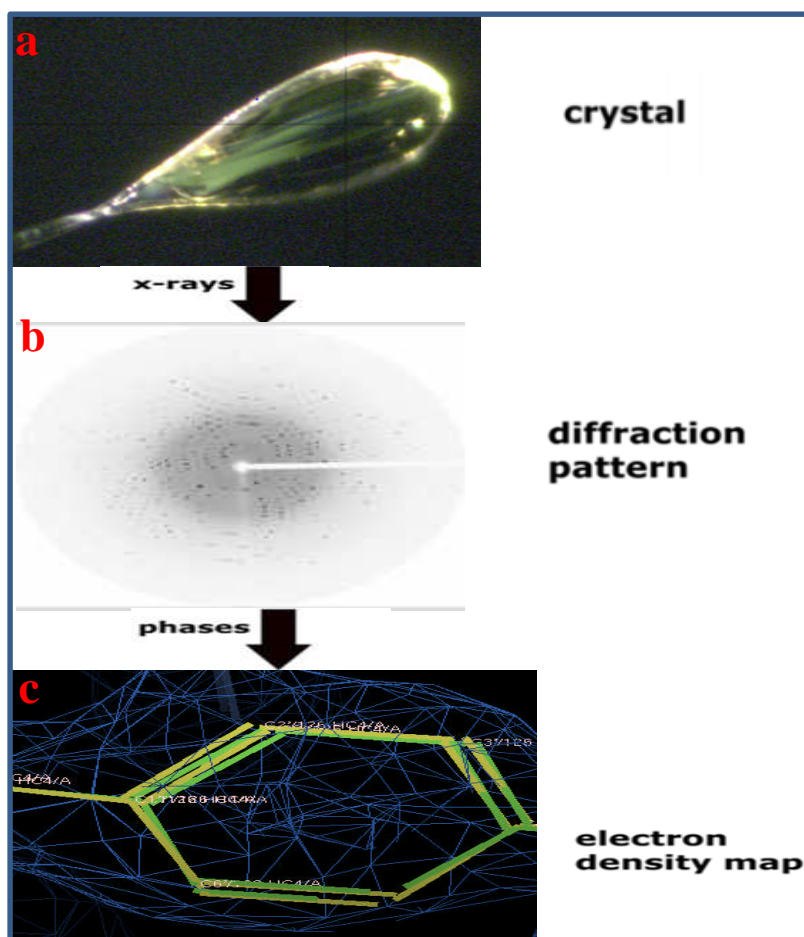


Figure 3-1: (a) PYP crystal mounted by cryoloop (b) Diffraction pattern collected from the MarCCD detector (c) Electron density map.

3.2 Data reduction

The diffraction data are processed to yield a file of intensities with their standard deviation and h, k, l indices. The process of determining the orientation, unit cell parameters, and space group and assigning the indices is called indexing. After collecting raw diffraction images, the intensities of the different peaks are determined (along with their standard deviation) in a process known as integration. Scaling which follows integration, determines a number of scale factors that place the intensities on a common scale. After that, the intensities are merged to produce an estimated average intensity (N. Chandra, 2013).

The initial indexing estimates of crystal orientation, cell dimensions, mosaicity, and beam position are refined during the scaling step. An accurate estimation of the direct X-ray beam position on the detector is essential because it corresponds to the origin of the reciprocal lattice. Data quality is indicated at this stage by a statistical measure such as R_{merge} and $I/\sigma(I)$ (N. Chandra, 2013). The scaling is done by merging to yield a file of the unique reflection intensities and standard deviations.

3.3 Phase determination

The structure factor can be represented as a vector or a complex number F_{hkl} with amplitude $|F_{hkl}|$ and phase φ_{hkl} . The phase is a major problem in X-ray crystallography. The X-ray detector (MarCCD) is only able to record intensities; the phases are not determined. The amplitude can be calculated by taking the square root of the intensity, but the phase is lost. However, the phase necessary to determine an electron density distribution (N. Chandra, 2013).

3.4 Crystallographic Object-Oriented Toolkit (COOT)

The coot software is used to obtain the electron density map. Coot (Crystallographic Object-Oriented Toolkit) is a molecular-graphics application for model building and validation of biological macromolecules (CCP4 manual). The program displays electron-density maps and allows model manipulations such as idealization, real-space refinement, manual, rotation/translation, rigid-body fitting, ligand search and finding water molecules (CCP4 manual). The software is under rapid development, but has already achieved very widespread use within the crystallographic community.

In recent years, initial construction of the protein chain has often been carried out using automatic model-building tools such as ARP/wARP (Langer *et al*, 2008), SOLVE/RESOLVE (Wang *et al*, 2004) and, more recently, Buccaneer (R. Cowtan, 2006). The refinement and validation steps become increasingly important as well as more time-consuming, with lower resolution data (CCP4 manual). Coot aims to provide access to many of the tools required in the iterative refinement and validation of a macromolecular.

3.5 Refmac

Coot provides interfaces to external programs. Interfaces to REFMAC and SHELXL (F. Sheldrick, 2008) are provided for refinement. I used only the REFMAC tool. Coot provides a dialogue similar to that used in CCP4i for running REFMAC (Murshudov *et al*, 2004). REFMAC is a program from the CCP4 suite for maximum-likelihood-based macromolecular refinement (CCP4 manual). Reflections for the refinement are either used from the MTZ (compressed metastream scene) file from which the currently displayed map was calculated or can be acquired from a selected MTZ file (CCP4 manual). Most

REFMAC parameters are set as defaults; however, some, such as the number of refinement cycles, can be specified in the Graphical user interface. Once REFMAC has terminated, the newly generated (refined) model and MTZ file from which maps are generated are automatically read in (and displayed) (CCP4 manual). If REFMAC detects geometrical outliers at the end of the refinement, an interactive dialogue will be presented.

Chapter 4

Results

Introduction

In Chapter 4, the results of X-ray diffraction pattern for PYP and ccNiR are described in detail. Statistics of the PYP data collected at room and low temperatures are given in detail in Table 4.3.1.

4.1 X-ray diffraction pattern for PYP

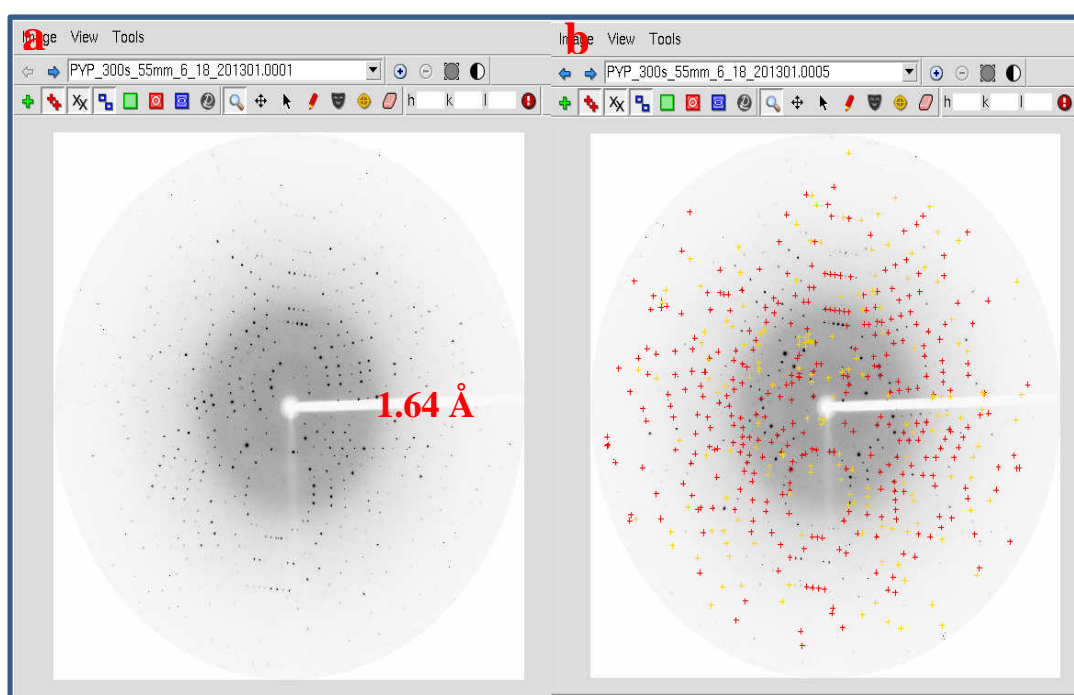


Figure 4-1: A typical diffraction pattern for a strongly diffracting crystal is shown on the left; the detected reflections are shown on the right. Each reflection is noted by a cross-hair, with red and yellow used to denote those reflections above and below the current threshold used for indexing, respectively.

Imosflm is used to determine the reflection of intensity from the diffraction pattern. Figure 4.1(a) shows the lower intensity in gray and the higher intensity in black; Figure 4.1(a) shows the diffraction pattern in which the data was collected at a low temperature (100° k),

and the resolution obtained is 1.64 Å. The software denotes detected reflections by red and yellow crosshairs. Red crosshairs are for those reflections above the currently defined threshold, and yellow crosshairs are for those reflections below. In PYP crystal, the reflections of intensity are well separated.

4.2 X-ray diffraction pattern for ccNiR

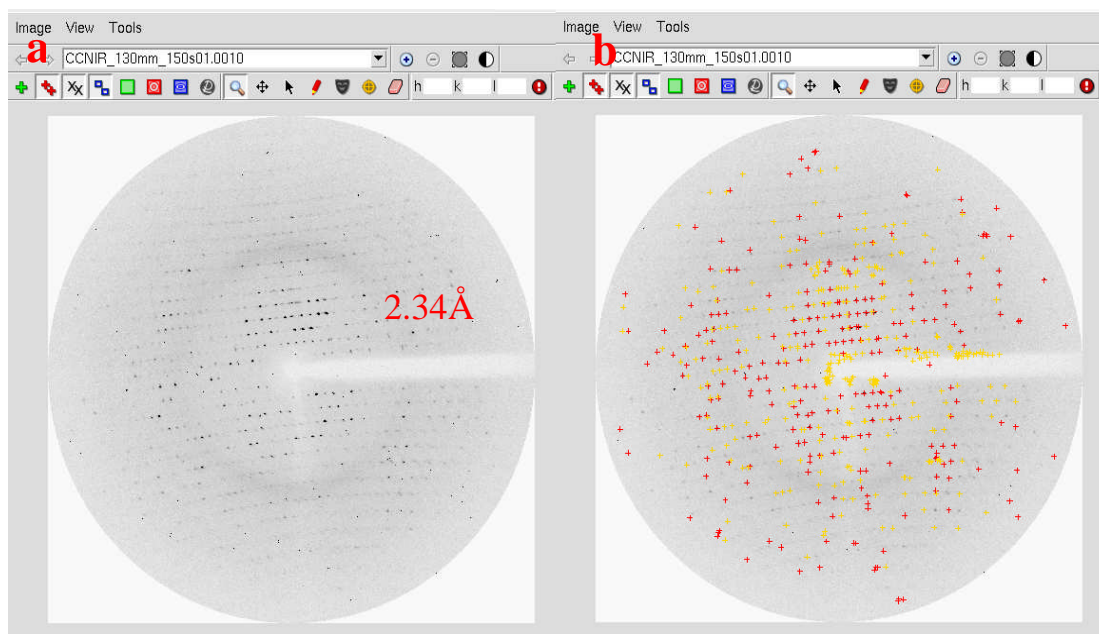


Figure 4-2: A typical diffraction pattern for a strongly diffracting crystal is shown on the left; the detected reflections are shown on the right. Each reflection is noted by a cross-hair, with red and yellow used to denote those reflections above and below the current threshold used for indexing, respectively.

Imosflm is used to determine the reflection of intensity from the diffraction pattern. Figure 4.2(a) shows lower intensity in gray and the higher intensity in black. For the diffraction pattern in which the data was collected at a low temperature (100°k) the resolution obtained is 2.34 Å. Each reflection of the diffraction pattern is not properly fit with the intensity in the imosflm software. In ccNiR crystals, reflections of intensity are not well separated.

There are a couple of factors that make ccNiR difficult to measure. One of these reasons is that ccNiR does not like to be frozen. This means that its mosaicity suffers at cryo temperatures, but ccNiR is also highly susceptible to radiation damage, which makes monochromatic data difficult to obtain at room temperature. Also, the Laboratory Microfocus X-ray Source for Protein Crystallography (LMXS-PC) facility has a larger beam divergence than the APS (Advanced Photon Source). Indexing proved troublesome because the reflection spots were difficult for imosflm to separate. The reason I moved the detector back was a purely geometrical one: moving the detector back allowed the reflections more distance to spread out.

4.3 Data statistics

4.3.1 Table 1: Data statistics for PYP

The table below gives the details of the data collection done for PYP crystals in temperatures of 100°k and 273°k.

Parameter	100°k	273°k
Wavelength(Å)	1.54	1.54
Space group	P63	P63
Cell dimension(Å)	a=b=65.78,c=40.28	a=b=66.82,c=40.79
Low resolution range(Å)	16.44	16.70
High resolution range(Å)	1.64	1.64
No of observations	52507	51362
No of unique reflection	12204	12108

Mosaicity	0.48°	0.35°
I/ σ (I)	28.7	15.8
Completeness (%)	99.7	94.4
R _{merge} (%)	2.5	4.2
Maximum resolution(Å)	1.64	1.64

4.4 Electron density map for PYP

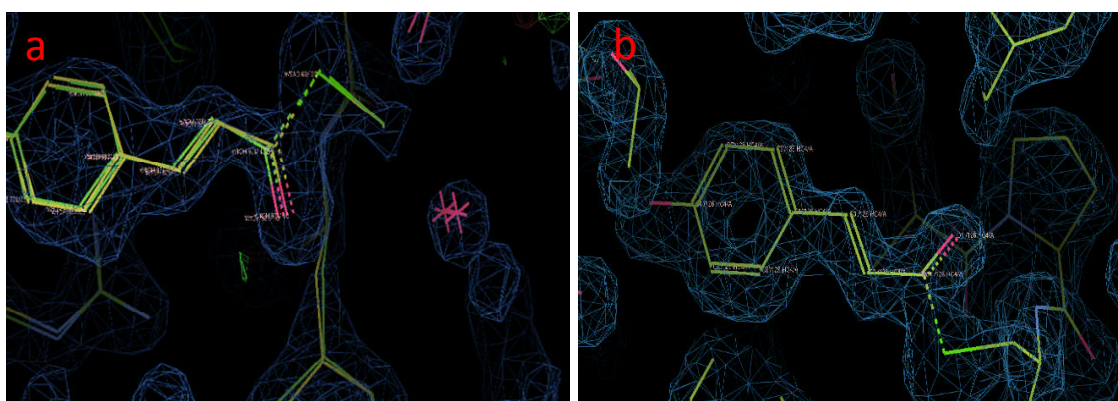


Figure 4-3: (a) Electron density map obtained using the COOT software for low temperature data set (b) Electron density map obtained using the COOT software for room temperature data set (screen shot).

4.4.1 Low temperature

The resolution I can obtain with the LMXS-PC facility is 1.53 Å. X-rays were data collected using crystals in a cryoloop at 100°k. Data were integrated and scaled with the HKL package (Otwinowski & Minor, 1997). The crystal belonged to the hexagonal space

group P63, with unit-cell parameters $a = b = 65.75$, $c = 40.28$. Further details of the data collection statistics are presented in Table 4.3.1.

4.4.2 Room temperature

The X-ray diffraction experiments were performed at LMXS-PC built X-ray source at room temperature (273°K). The crystal was mounted using the Mitegen loop method. The diffraction data were recorded with a MarCCD (165mm) detector over a rotation of 75° with steps of 0.5°. The wavelength was set to 1.54 Å; the detector distance and exposure time were 55mm and 300s respectively. The detailed procedure is explained in Section 7 of the Appendix IV.

The refinement programs were used to refine the structural model, and Coot was used to build the model (P. Emsley, 2004). During the analysis, several residues were found to occupy more than one conformation; these multiple conformations were subsequently built and refined (P. Emsley, 2004). The final values of R_{merge} were 4.2%. Model quality was implemented in CCP4 (Collaborative Computational Project, Number 4, 1994); the detailed statistics of data collection are shown in Table 4.3.1.

Chapter 5

Discussion

5.1 Discussion

This section of the thesis gives a brief summary, discussion and the analysis of the data obtained from the Laboratory Microfocus X-ray Source for the Protein Crystallography (LMXS-PC) set-up. In summary, I have contributed to stepper motor controller for the goniometer axis and to image processing to measure crystal size (programmatic control and remote capability) for the LMXS-PC safe X-ray source. In addition, I have validated its functionality by analyzing data collected for PYP and ccNiR crystals.

Diffraction experiments were performed at two different temperature settings. The data were collected at 100°K and 273°K using a MarCCD detector. The other configurations of the set-up, such as sample to detector distance (55mm), exposure time (300s), and width (0.5mm), remained the same for the two cases. The cell dimensions at both temperatures are shown in Table 4.3.1.

The difference in data collected at the two temperatures can be observed in the R_{merge} , completeness and mosaicity listed in table 4.3.1. The low R_{merge} value at 100°K corresponds to better quality data, although the obvious limitation is that R_{merge} increases with increasing redundancy, even though higher redundancy generally gives better data (E.I. Master, 2008). The higher mosaicity at the low temperature might explain why reflections start to overlap in the diffraction pattern. This, in turn may affect the quality of extracted intensities.

Considering the LMXS-PC in relation to other crystallography instruments, image collection is one point of distinction. Image plates have a long history of use in X-ray crystallography. Image plates can be large, they are sensitive and have large dynamic

range. The problem with the image plate is that it takes a long time to read the data. But this is not a significant issue with LMXS-PC data collection, where exposure times are usually between 15-60 minutes per image.

The CCD detectors used at synchrotrons are relatively sensitive area detectors with a reasonable dynamic range and fast readout time. They usually occupy a smaller area than an image plate and have a much faster readout time, which is an advantage at a synchrotron; where typical, exposure times are between 5-40 seconds.

The best resolution I obtained with the LMXS-PC facility is 1.52 Å. This depends on multiple factors, one being the wavelength of the X-ray radiation emitted (1.54 Å LMXS-PC facility). Another factor is the closest distance the detector may be brought to the sample (45mm of the LMXS-PC facility). These factors limit resolution, regardless of the protein being studied. The resolution limit of the LMXS-PC is near 1.52 Å, which is near the resolution limit. The APS (Advanced Photon Source, synchrotron in Argonne, Illinois) has a more intense beam and higher energy (shorter wavelength), so it has the ability to obtain a greater resolution of 0.8 Å.

LMXS-PC has a small focal spot size compared to the rotating anode X-ray generator, which is described in the tables 7.8.1 and 7.8.3. The average power of the synchrotron, described in tables 7.8.2 and 7.8.3, is much higher than that of the LMXS-PC. For brilliance the LMXS-PC and rotating anode generator are very similar, while the synchrotron is three times more brilliant than the other two.

Possible future work includes further validating the LMXS-PC safe X-ray source using a ccNiR crystal. This will require the use of a more effective techniques for growing ccNiR crystals, which should in turn provide better data sets and improved resolution.

5.2 Conclusion

In conclusion, I contributed to a crystal alignment tool with remote control. The user can simply mount the crystal in the X-ray instrument and operate it from anywhere through the TCP/IP protocol. The ability to adjust orientation at a distance reduces the exposure of the operator to X-rays.

The primary function of the camera program is to measure the crystal size. While many different programs are available for this purpose, the one I used is simple, and user friendly.

The buffer solution was prepared to keep the crystal within the loop until the data is collected. The chemical compound (Section 2.4.1) mentioned in this thesis worked successfully with the PYP crystal. The best resolution I could obtain with the LMXS-PC was 1.52 Å. This result lies in the resolution range (1.2-1.54 Å) reported by Galburt who also used a monochromatic X-ray source (E.A. Galburt, 2001).

6 References

1. T. E. Meyer, Yakali, M. A. Cusanovich and G. Tollint, "Properties of a Water-Soluble, Yellow Protein Isolated from a Halophilic Phototrophic Bacterium That Has Photochemical Activity Analogous to Sensory Rhodopsin," *Biochemistry*, 26(2):418-423, 1987.
2. Maria Gabriela Almeida, Sofia Macieira, Luisa L.Gonc, alves, Robert Huber, Carlos A. Cunha, Maria Joao Romao, Cristina Costa, Jorge Lampreia, Jose J.G.Moura and Isabel Moura, "The isolation and characterization of cytochrome c nitrite reductase subunits (NrfA and NrfH) from *Desulfovibrio desulfuricans* ATCC 27774," *Biochemistry*, 270(19):3904-3915, 2003.
3. Youngblut M, Judd ET, Srajer V, Sayyed B, Goelzer T, Elliott SJ, Schmidt M, Pacheco AA, "Laue crystal structure of *Shewanella oneidensis* cytochrome c nitrite reductase from a high-yield expression system," *Journal of Biological Inorganic Chemistry*, 17(4):647-662, 2012.
4. Yevgeniy Kalinin, Jan Kmetko, Adam Bartnik, Andrew Stewart, Richard Gillilan, Emil Lobkovskyd and Robert Thorne, "A new sample mounting technique for room temperature macromolecular crystallography," *Journal of Applied Crystallography*, 38(2):333-339, 2005.
5. Cohen, A.E., Ellis, P.J., Miller, M.D., Deacon, A M and Phizackerley, R.P, "An automated system to mount cryo-cooled protein crystals on a synchrotron beamline, using compact sample cassettes and a small-scale robot," *Journal of Applied Crystallography*, 35(6):720-726, 2002.

6. S. M. Soltis, A. E. Cohen, A. Deacon, T. Eriksson, A. Gonzalez, S. McPhillips, H. Chui, P. Dunten, M. Hollenbeck, I. Mathews, M. Miller, P. Moorhead, R. P. Phizackerley, C. Smith, J. Song, H. van dem Bedem, P. Ellis, P. Kuhn, T. McPhillips, N. Sauter, K. Sharp, I. Tsyba and G. Wolf, "New Paradigm for Macromolecular Crystallography Experiments at SSRL: Automated Crystal Screening and Remote Data Collection," *Acta Crystallographica*, 64(12):1210-1221, 2008.
7. Daan M. F. van Aalten, Wim Crielaard, Klaas J. Hellingwerf and Leemor Joshua-Tora W. M. Keck, "Structure of the photoactive yellow protein reconstituted with caffeic acid at 1.16 Å resolution," *Acta Crystallographica*, 8(4):585-590, 2002.
8. Duncan E. Mcree, John A. Tainer, Terry E. Meyer, Josef Van Beeumen, Michael A. Cusanovicht and Elizabeth D. Getzoff, "Crystallographic structure of a photoreceptor protein at 2.4 Å resolution," *Proceedings of the National Academy of Sciences*, 86(9):6533-6537, 1989.
9. M. D. Winn, A. W. Ashton, P. J. Briggs, C. C. Ballard and P. Patel, "Ongoing developments in CCP4 for high throughput structure determination," *Acta Crystallographica*, 58(11):1929-1936, 2002.
10. Yang Ouk Jung, Jae Hyuk Lee, Joonghan Kim, Marius Schmidt, Keith Moffat, Vukica Šrajer & Hyotcherl Ihee, "Volume-conserving trans-cis isomerization pathways in photoactive yellow protein visualized by picosecond X-ray crystallography," *Nature Chemistry*, 5(3):212-220, 2013.
11. Paul Emsley and Kevin Cowtan, "Coot: model-building tools for molecular," *Acta Crystallographica*, 60(12):2126-2132, 2004.

12. Ulrich K. Genick, S. Michael Soltis, Peter Kuhn, Ilona L. Canestrelli & Elizabeth D. Getzoff, "Structure at 0.85 Å resolution of an early protein photocycle intermediate," *Nature*, 392(6672):206-209, 1998.
13. Longley. W, "A simple rotating anode X-ray generator," *Review of Scientific Instruments*, 46(1):30-32, 1975.
14. Bykov, D., and Neese, F, "Substrate binding and activation in the active site of cytochrome c nitrite reductase: a density functional study," *Journal of Biological Inorganic Chemistry*, 16(3):417-430, 2011.
15. T. E. Meyer, G. Tollin, J. H. Hazzard, and M. A. Cusanovich, "Photoactive yellow protein from the purple phototrophic bacterium, *Ectothiorhodospira halophila*," *Journal of Biophysics*, 56(3):559-564, 1989.
16. McRee, D. E., Meyer, T. E., Cusanovich, M. A., Parge, H. E. & Getzoff, E. D, "Crystallographic structure of a photoreceptor protein at 2.4 Å resolution," *Proceedings of the National Academy of Sciences*, 86(17):6533-6537, 1989.
17. Jose Trincao, Michelle L. Hamilton, Jeppe Christensen, Arwen R. Pearson, "Dynamic structural science: recent developments in time-resolved spectroscopy and X-ray crystallography," *Biochemical Society Transactions*, 41(5):1260-1264, 2013.
18. P. Emsley, B. Lohkamp, W. G. Scott and K. Cowtan, "Features and development of Coot," *Acta Crystallographica*, 66(4):486-501, 2010.
19. K. Cowtan, P. Emsley and K. S. Wilson, "From crystal to structure with CCP4," *Acta Crystallographica*, 67(4):233-234, 2011.

20. Andrew G.W. Leslie, Harold R. Powell, "Processing diffraction data with mosflm," *NATO Science Series*, 245(5):41-51, 2007.
21. Battye TG, Kontogiannis L, Johnson O, Powell HR, Leslie AG, "iMOSFLM: a new graphical interface for diffraction-image processing with MOSFLM," *Acta Crystallographica D Biological Crystallographica*, 67(4):271-281, 2011.
22. R.A.Crowther, ed. M.G. Rossman, "The Fast Rotation Function in the Molecular Replacement Method," *Review of scientific instruments*, 13(8):173-178, 1972.
23. Beliaev, A. S., Klingeman, D. M., Klappenbach, J. A., Wu, L., Romine, M. F., Tiedje, J. M., Nealson, K. H., Fredrickson, J. K., and Zhou, J, "Global Transcriptome Analysis of *Shewanella oneidensis* MR-1 Exposed to Different Terminal Electron Acceptors," *Journal of Bacteriology*, 187(20):7138-7145, 2005.
24. Meyer, T. E., Tsapin, A. I., Vandenberghe, I., de Smet, L., Frishman, D., Nealson, K. H., Cusanovich, M. A., and J.J., v. B, "Identification of 42 possible cytochrome c genes in the *Shewanella oneidensis* genome and characterization of six soluble cytochromes," *A Journal of Integrative Biology*, 8(1):57-77, 2004.
25. Einsle, O., Messerschmidt, A., Stach, P., Bourenkov, G. P., Bartunik, H. D., Huber, R., and Kroneck, P. M. H, "Structure of cytochrome c nitrite reductase," *Nature*, 400(6743):476-480, 1999.
26. Dr. Naba K. Nath, Dr. Kochunnonny Manoj, Dr. Andrei Șerban Gâz, Prof. Panče Naumov, "Visible-Light-Induced Photodimerization of a Photoactive Yellow Protein (PYP) Chromophore Model in a Single Crystal," *A European Journal*, 19(25):8094-8099, 2013.

27. Kroon AR, *et al.*, "Spectral tuning, fluorescence, and photoactivity in hybrids of photoactive yellow protein, reconstituted with native or modified chromophores," *Journal of Biological Chemistry*, 271(50):31949-31956, 1996.
28. Keisuke Saito and Hiroshi Ishikita, "Energetics of short hydrogen bonds in photoactive yellow protein," *Proceedings of the National Academy of Sciences*, 109(1):167-172, 2011.
29. D.Bourgeois, U.Wagner, and M.Wulff, "Towards automated Laue data processing: application to the choice of optimal X-ray spectrum," *Acta crystallographica*, 56(8):973-985, 2000.
30. Rupp, B, "Biomolecular crystallography," Garland Science, 2(7):205-208, 2009.
31. Drenth, J, "Principles of Protein X-ray Crystallography," Springer, 3(19):534-537, 1995.
32. Namrta Purwar, "Structure and function of proteins investigated by crystallographic and spectroscopic time-resolved methods," Ph.D. dissertation, Dept. Physics, University of Wisconsin-Milwaukee, Milwaukee, WI, 2013.

7 Appendix

7.1. Turning on micro focus X-ray source

1. First the vacuum pump is switched on.
2. Once the vacuum pump is on, check the chiller temperature and the level of fluid.
3. Once both are stable, and then turn on the chiller by pressing the on/off switch.
4. Wait for some time before turning on the X-ray control unit.
5. Once the chiller is ready and then turns on the X-ray control unit by pressing the ON button.
6. The display screen appears, and then press the R6 button and then new window pop-up.
7. Press the X-ray button on.
8. Turn the X-ray key to the on position.
9. In the display screen touch the start cycle. The voltage and the current starts increase and reach to the user required voltage and current.
10. Once the users see the voltage (50V) and the current (1mA) and wait still it is fully power up and reliably stable.
11. Press the safety shutter and then the fast shutter.
12. X-ray is ready to expose the crystal.

7.2. Turning off micro focus X-ray source

1. First press the power down cycle in the display screen.
2. The voltage and current must start to go down and reach the value zero.
3. Turn the key towards the off position,
4. Now it is ready to press the off button and the X-ray control unit is completely off.
5. Wait for some time before turning off chiller, so the X-ray machine cool down
6. Turn off the chiller by pressing the off button and it is finally safe to turn the vacuum off.
7. Now everything is shut off.

7.3. Using the Cryojet

1. Fill the nitrogen tank and connect the dewar and nitrogen tank using the hose.
2. Turn on the valve in the nitrogen tank.
3. Press the power button on in the cryojet controller.
4. The level of nitrogen is adjusted by the user manually.
5. Once the dewar filled then set the temperature based on user need in the experiment.
6. Next step is set the shield and sample flow it also depend on user need.
7. Turn on heater at the end.

8. After data collected, the temperature is set to 300k and once it reaches the temperature.
9. The cryojet is turned off and close the valve in the nitrogen cylinder.

7.4. Sample Preparation for Cryobuffer

The chemical compound that need for preparing cryobuffer are 3.2M of Ammonium Sulphate, 300mg/ml of sugar or sucrose, 15% of glycerol and 50mmol of $\text{Na}_2\text{H}_2\text{PO}_4$ (monobasic)(monohydrate) for 50ml of water.

Calculation

$$(i) \text{ 3.2M of Ammonium Sulphate [g]} = 3200 \text{ m mol/L} * 132 / (1000 * 1000) * 50 \text{ ml}$$

$$= 21.12 \text{ g of ammonium sulphate}$$

$$(ii) \text{ 300mg/ml of sugar or sucrose} = 300 \text{ mg/ml} * 50 \text{ ml}$$

$$= 15 \text{ g of sugar}$$

$$(iii) \text{ 15\% of glycerol} = 50 \text{ ml} * 15 / 100$$

$$= 7.5 \text{ ml of glycerol}$$

$$(iv) \text{ 50mL of } \text{Na}_2\text{H}_2\text{PO}_4 = 137.99 / 10^6 * 50 * 50 \text{ mmol/L}$$

$$= 0.34 \text{ g or } 344.975 \text{ mg of } \text{Na}_2\text{H}_2\text{PO}_4$$

Procedure for preparing the cryobuffer

- (i) Weight correct amount of all chemical compound in a weighing machine.
- (ii) After weighing add all compounds in a clean glass beaker.

- (iii) Add 25-30ml of ionized water in the beaker.
- (iv) Put the stirrer inside the beaker and cover the top of beaker with filter paper (4.5um).
- (v) Check all the chemical compounds are dissolved otherwise keep adding ionized water still all compounds are dissolved and never exist the limit of ionized water.
- (vi) Stop stirring when we see nice transparent inside the beaker.
- (vii) Then set pH to 7.
- (viii) Pour the solution into the graduated cylinder.
- (ix) And make up to the volume of 50ml of ionized water.

Checking the pH value

- (i) Calibrate the pH meter of known (pH 7).
- (ii) In the glass beaker put the pH sterilizer and measure the pH.
 - (a) If the $\text{pH} < 7$, then add NaOH (10 mol/L).
 - (b) If the $\text{pH} > 7$, then add HCl (30% of concentration).

Then pour the solution in the graduated cylinder. Take the syringe and attach the filter top of it. Now suck the solution and squeeze into the clean air tight container bottle and finally label the bottle with the all compound that needed to prepare the cryobuffer solution.

7.5. Detailed procedure for collecting data set

Screening crystals for diffraction

The following steps must be carried out prior to commencing data collection:

- The X-ray source make sure that the X-ray beam is not on and the shutter is not open and immediately verify that the X-ray shutter is manually closed. Closing the shutter minimizes the risk of being exposed to direct or backscattered X-ray radiation while working with the system.
- Immediately before collecting data, energize the X-ray source by increasing the voltage to 50 kV and increasing the current to 1 mA. These steps should be carried out in this order, and it is precautionary to increase both settings gradually as you bring up the source.

Collecting diffraction screen data

The following steps are typical for collecting crystal screens:

- Fill them with liquid nitrogen.
- Obtain an empty crystal cap and loop the same size and type as those you will be using for data collection.
- Move the cryojet head back to allow sufficient clearance for mounting crystals on the goniometer without touching the X-ray source, beam stop, or cryojet head.
- Mount the empty crystal cap and loop on the goniometer head and adjust the height so that the loop is centered in the X-ray beam and cryojet. Remove the empty cap and loop when adjustments have been completed.

- Immediately adjust the goniometer head so that the crystal is centered vertically in the beam and properly centered in the cryostream.
- Unlock the ϕ -axis of the goniometer and swing it to 0° . Adjust the goniometer using the SMC crystal alignment tools until it is centered in the beam. Swing the goniometer to 90° and repeat. Do the same for 180° and 270° orientations. Repeat as necessary until the crystal is centered in the beam and rotates without wobbling in the center of the X-ray beam. You can check the accuracy of your alignment by looking for lateral displacement when the goniometer head is swung 180° : i.e., you should check that the crystal is not laterally displaced when swung 0 - 180° or 90 - 270° .
- Switch the X-ray shutter from closed to external and close the door.
- Start the data collection software by entering the time, width and total number of frames in the MarCCD software.
- Enter your data collection parameters. For screening crystals it is useful to shoot three frames at 0° , 45° and 90° rotation about the ϕ -axis to evaluate diffraction along different crystal axes. This distance is sufficient to collect data to 2.5 \AA at the edge of the frame. Exposure times per frame of 2-20 minutes are also based on prior to user desired time.
- Initiate data collection.
- Individual frames should be analyzed by imosflm for indexing and preliminary assignment of space group as described in the section on X-ray diffraction data analysis.
- Perform the appropriate shutdown procedures

Shutdown Procedure

The X-ray diffractometer should be shut down in order to maximize the life of the X-ray source.

- Ensure that data collection has stopped. If necessary use stop data collection manually using the emergency stop button in the data collection software. Do not go near the X-ray source until you have verified that the X-ray beam shutter has been closed.
- Return the X-ray source to minimum power by turning the current down to the minimum level, and then turning the voltage down to the minimum level.

Move the cryojet head back to allow sufficient clearance for removing crystals from the goniometer without touching the X-ray source, beam stop or cryostream head.

- Unlock the ϕ -axis of the goniometer and swing it to an angle where the notch on the crystal cap will line up with the notch on the cryojet when they are used to remove to crystal.
- Shut down the cryojet controller by setting the temperature to 300k and attach the house nitrogen line to the Cryojet head. This will prevent condensation and ice formation in the cryojet head.

7.6. Imosflm

Steps involved in the imosflm

The Data reduction done using the Imosflm software. The following steps are done:

(i) Images

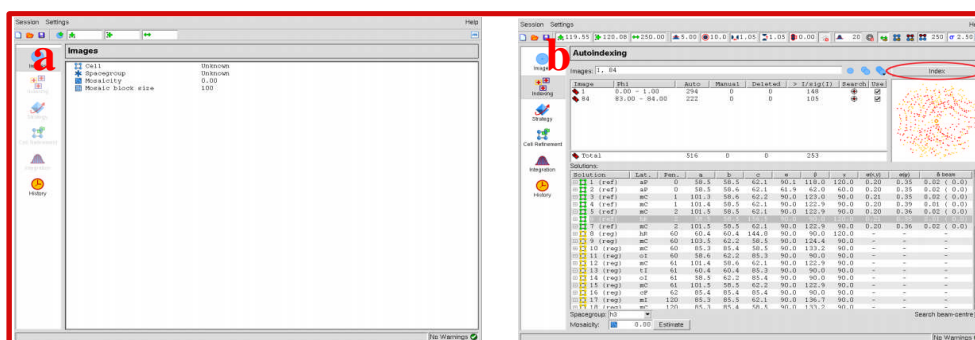


Figure (i) (a): Display of the imosflm from imosflm manual (b) Display of the index from imosflm manual.

The operations listed down the left hand side can be selected by clicking on the appropriate icon shown in the figure (i) (a). Then click on session a drop down menu appear which will allow to add new images.

Select the correct directory from the pop-up Add Images window. Double-clicking on any file will result in all images with the same template being added to the session (imosflm manual). An alternative is to single-click on one image filename and then click on Open in the directory.

(ii) Indexing

If there are no errors in showing the spot finding, then indexing will be carried out automatically after spot finding. If the image selection or indexing parameters are changed, the Index button must be used to carry out the indexing (imosflm manual). At this point it will automatically estimate the mosaic spread (mosaicity).

The indexing is very sensitive to errors in the direct beam coordinates. For a correct indexing solution, these should be correct to better than half the minimum spot separation (imosflm manual).

The indexing will be carried out for each set of starting coordinates and if a solution is found the refined beam coordinates the unit cell parameters. To complete the indexing, double-click on the chosen solution, and the full indexing will carried out for these beam coordinates (imosflm manual).

Mosaicity

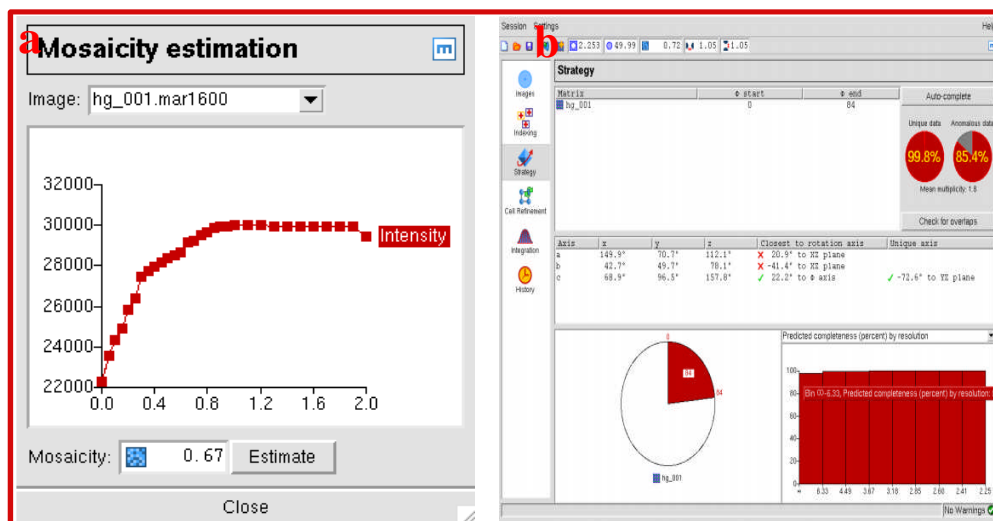


Figure (ii) (a): Display of the mosaicity from imosflm manual (b) Display of the strategy from imosflm manual.

The mosaicity (mosaic spread) will be estimated automatically for the preferred solution. However, if another solution is chosen, the mosaicity should be estimated again. Click on the Estimate button to estimate the mosaicity as shown in the figure (ii) (a). A window will appear which plots the total predicted intensity as a function of mosaic spread, from which an estimate is determined (imosflm manual).

The predictions displayed on the image will be updated. Entering different values of mosaic spread in the box (followed by return) will allow a visual estimate of the effect of changing the mosaic spread (imosflm manual). The mosaic spread can also be defined in the Images pane.

In some cases, the apparent mosaic spread is much larger at low resolution than at high resolution, so that if it is set to a value that results in all the low resolution spots being

predicted, many more spots are predicted than are visible at high resolution (imosflm manual). This effect is best dealt with by adjusting the mosaic block size which is also displayed in the Images pane. This is modelling the size, in microns, of the individual mosaic blocks in the crystal.

(iii) Strategy

Once the crystal orientation have been determined, it is possible to calculate a data collection strategy. Select the Strategy icon. This will open the Strategy window.

The Strategy option will be used after two initial images, 90° apart in ϕ , have been collected, and the statistics will represent the completeness of that 90° of data (imosflm manual). The orientation of the crystal, expressed as the angles between a, b, c unit cell.

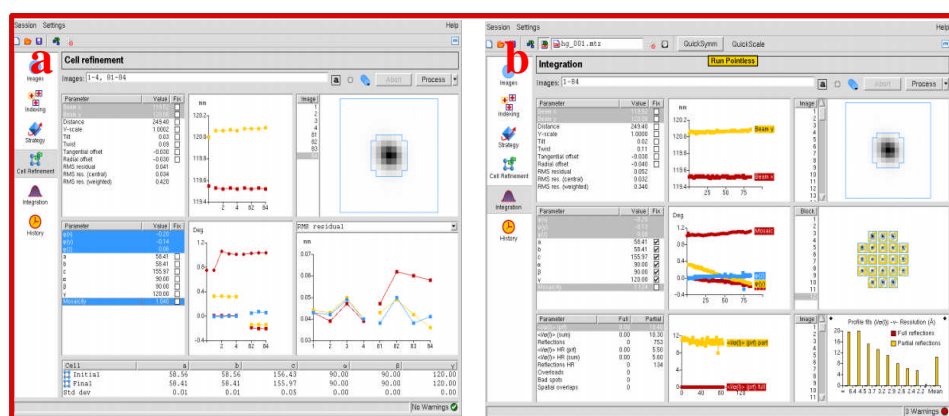


Figure (iii) (a): Display of the cell refinement from imosflm manual (b) Display of the integration from imosflm manual.

(iv) Cell Refinement

It is important to determine the cell parameters accurately before integrating the images. Although the unit cell is refined as part of the auto indexing, providing the diffraction, it is possible to obtain more accurate cell parameters using a procedure known as post-

refinement(imosflm manual). This procedure requires the integration of a series of images in ideally two or more separate segments at widely different ϕ values (imosflm manual). The distribution of the intensity of partially recorded reflections over the images on which they occur is used to refine the unit cell, crystal orientation and mosaic spread (imosflm manual). Select the Cell refinement icon on the left side as shown in the figure above (iii) (a).

(v) Integration

The selected images will be integrated, and following integration the cell parameters are refined. Click on the Process button to start integration on the left side of the window as shown in the figure above (iii) (b). Integration of the images occurs in two things. In the first, each block of images (typically 5-10, selected automatically by MOSFLM), the detector and crystal parameters are refined for each image in turn and the boxes for all predicted spots are written to a file for use in the second (imosflm manual). In the second, the standard profiles are formed from reflections present on all of the images in this block, and each image is then integrated and the results written to the MTZ file (imosflm manual).

7.7. CCP4

Introduction about CCP4

The Collaborative Computational Project Number 4 (CCP4) supports the development and use of software in macromolecular crystallography (Collaborative Computational Project, Number 4, 1994; Dodson et al., 1997). However, CCP4 programs do feature in many such protocols and therefore CCP4 has an important role in providing the correct tools for high-

throughput studies. Recent examples of procedures based at least partly around CCP4 programs include the validation script developed by (Badger & Hendle 2002) and the Elves automated structure solution package (Holton, 2002). The individual programs of the CCP4 software suite provide the essential functionality for structure solution (CCP4 manual).

(i) *Project & Directories*

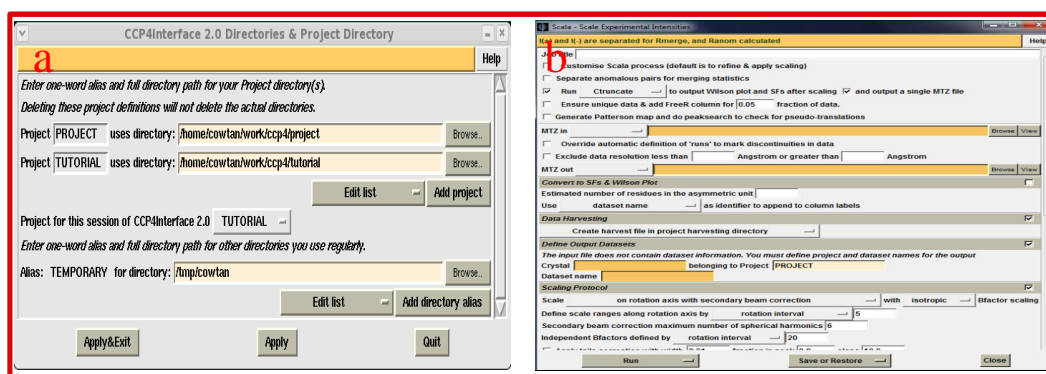


Figure (i) : (a) *Creating the project & Directories from CCP4 manual* (b) *creating the scala from CCP4 manual.*

The first time you run the Interface, the window which enables you to set up directory aliases and define a project directory comes up automatically (CCP4 manual). The window will appear as shown in the figure above (i) (a).

The CCP4 Interface is designed with the expectation that all data files relating to one crystallographic project will be in one directory. It is simple to override this but it may be helpful to organize all CCP4 work this way (CCP4 manual). You may have more than one project, and it is easy to switch between projects inside the Interface.

In the Directories & Project Dir window, enter one-word and the full pathname for the directories you use regularly. These directories can then be accessed quickly when

selecting files via a menu that lists your directory and goes straight to the directory you choose (CCP4 manual).

(ii) Scala

After creating the directories based on user needs to save as much information in the file name. The window will appear as shown in the figure above (i) (b). Then click on the refinement tool in the left side of window which enables you to set up the scala and also include necessary information (CCP4 manual). Then creating the job title and in the run selecting tool to run as an old truncate. The mtz file is given as the input which is generate from the imosflm.

The important things about this software the cell constant are automatically produced from the imosflm software (CCP4 manual). By saving the correct path it will automatically get all information from the imosflm software. Then clicking the run now button it gives the output in the scala of mtz file. At the end of the logfile there is a summary table which contains the information useful for deposition and n view logfile and click on show summary.

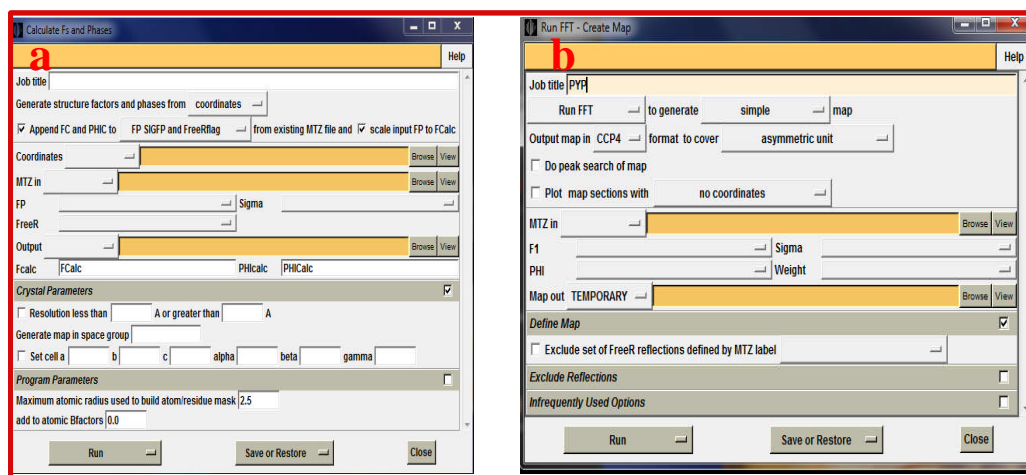
(iii) Sfall

Figure (ii): (a) Creating the sfall from CCP4 manual (b) Creating the fft from CCP4 manual.

After generating the scala and next step is creating the sfall. The window will appear as shown in the figure (ii) (a). Then click on the refinement tool in the left side of window which allow you to set up the fft and also include necessary information.

This is an interface to the sfall program which generates Fcalc and PHCalc from either input coordinates or a map (CCP4 manual). You must give the name of an input coordinate or map file and also an MTZ file into which the calculated Fs and PHIs are added. By default the calculated Fs and PHIs will cover the same resolution range as the one already in the MTZ file (CCP4 manual).

The Protocol folder has the choice between generating structure factors from coordinates or a map (after which the files folder is adapted accordingly), and the option to scale the input Fp to the Fcalc (CCP4 manual).

After the protocol and files folders, the Crystal parameter' folder has the option of adapting resolution range, space group and/or cell parameters (CCP4 manual). The program parameters' folder allows the adaptation of Maximum atom radius used to build atom/residue mask and the amount to add to atomic B factors (CCP4 manual). Finally by the run button sfall is done. At the end of the logfile there is a summary table which contains the information useful for deposition and view logfile and click on show summary.

(iv) FFT

After generating the sfall and next step is creating the fft. The window will appear as shown in the figure above (ii) (b). By clicking the refinement tool in the left side of window which enables you to set up the sfall and also include necessary information.

An electron density map needs to be calculated. In the CCP4 Suite this is done with the Fast Fourier Transform program (CCP4 manual). If fft is run independently from programs/tasks like Refmac, special care needs to be taken in the choice of map output (CCP4 manual). The fft task is most easily performed inside the various program interfaces.

Here the nF1-mF2 map is used with multi-coefficient amplitudes for the Fourier transform, usually of the form [W] (SCALE1 F1 - SCALE2 F2), where W is a weight, and F1 and F2 are structure factors. SCALE1 and SCALE2 are scale factors chosen by the user (*e.g.* a 2FO-1FC map would have SCALE1="2" and SCALE2=1).

Table 7.8.1: Rotating anode X-ray generator

The specification of the rotating anode X-ray generator are listed below (Rigaku manual):

Specification	Optic	Value
Focal spot size(μm)	all optics	$\text{Ø} = 70$
Power(kW)	all optics	1.2
Beam size at sample(μm)	VariMax HF	208
	VariMax HF LFE	189
Divergence(mR)	VariMax HF	4.8
	VariMaxHF LFE	4.8
Flux at $\text{Ø} = 100 \mu\text{m}$ (photons/sec)	VariMax HF	6.38×10^8
	VariMax HF LFE	8.16×10^8
Fluence (photons/sec/ mm^2)	VariMax HF	7.80×10^{10}
	VariMax HF LFE	1.04×10^{11}
Brilliance (photons/sec/ mm^2/mR^2)	VariMax HF	3.39×10^9
	VariMax HF LFE	4.51×10^9

Where,

VariMax HF-Variance maximum high flux.

VariMax HF LFE- Variance maximum high flu life.

Table 7.8.2: Synchrotron

A detailed discussion of the properties listed below (Synchrotron manual):

Parameters	Value
Wavelength(A)	1-5
Peak power(GW)	37
Average power(W)	210
Photon beam size(FWHM)** (μm)	100
Photon beam divergence(FWHM)*** (μrad)	0.8
Bandwidth (FWHM) (%)	0.08
Coherence time (fs)	0.3
Pulse duration(FWHM) (fs)	100
Min.pulse separation**** (ns)	93
Max.number of pulse per train**** (#)	11500
Repetition rate**** (Hz)	5
Number of photons per pulse (#)	1.8×10^{12}
Average flux of photons (#/sec)	1.0×10^{17}
Peak brilliance (B*****)	8.7×10^{33}
Average brilliance (B*****)	4.9×10^{25}

where, *Parameters are given for the shortest wavelength.

** Value at the exit of the undulator.

*** Far field divergence.

**** Values determined by the time structure of the electron beam in the accelerator.

***** In units of photons/ (sec \cdot mrad² \cdot mm² \cdot 0.1 %bandwidth).

Table 7.8.3: Sealed tube

The maximum power loading and the respectively brilliance of a sealed X-ray tube (Rigaku manual):

Parameters	#1	#2	#3	#4	#5	#6	#7
Power(kW)	2	1.5	0.8	0.035	0.03	0.01	0.0012
e-beam incident angle(degrees)	90	90	90	90	78	45	90
Focal spot Length (mm)	10	8	8	0.2	0.14	0.02	0.002
Focal spot Width(mm)	1	0.4	0.15	0.02	0.02	0.0135	0.002
Takeoff angle(degrees)	6	6	6	6	8	45	6
Real power loading(kW/mm ²)	0.2	0.5	0.7	8.8	10.4	38.8	300.0
Calculated power loading(kW/mm ²)	0.3	0.7	1.5	16.6	18.2	49.1	391.5
Relative power loading(kW/mm ²)	0.60	0.67	0.44	0.53	0.57	0.79	0.77
Brilliance (photons/sec mm ² mrad ²)	5.8x 10 ⁷	1.4x 10 ⁷	1.9 x 10 ⁷	2.6 x 10 ⁷	2.6 x 10 ⁷	3.2 x 10 ⁷	9.2 x 10 ⁷